Bioorganic Chemistry 153 (2024) 107850

Contents lists available at ScienceDirect

Bioorganic Chemistry

journal homepage: www.elsevier.com/locate/bioorg

First dual inhibitors of human topoisomerase IIα and Hsp90 C-terminal domain inhibit the growth of Ewing sarcoma *in vitro* and *in vivo*

Jaka Dernovšek [a], Dunja Urbančič [a], Živa Zajec [a], Caterina Sturtzel [b], Sarah Grissenberger [b], Andrea Wenninger-Weinzierl [b], Marius Gedgaudas [c], Asta Zubrienė [c], Tjaša Goričan [d], Simona Golič Grdadolnik [d], Žiga Skok [a], Janez Ilaš [a], Martin Distel [b], Nace Zidar [a,*], Tihomir Tomašič [a,*]

[a] Faculty of Pharmacy, University of Ljubljana, Aškerčeva cesta 7, 1000 Ljubljana, Slovenia
[b] St. Anna Children's Cancer Research Institute, Zimmermannplatz 10, 1090 Vienna, Austria
[c] Department of Biothermodynamics and Drug Design, Institute of Biotechnology, Life Sciences Center, Vilnius University, Saulėtekio al. 7, LT-10257 Vilnius, Lithuania
[d] Laboratory for Molecular Structural Dynamics, Theory Department, National Institute of Chemistry, Hajdrihova 19, 1001 Ljubljana, Slovenia

ARTICLE INFO

Keywords:
Cancer
Ewing sarcoma
Hsp90
Inhibitor
Topoisomerase IIα
Zebrafish

ABSTRACT

Heat shock protein 90 (Hsp90) and topoisomerase IIα (TopoIIα) are members of the GHKL protein superfamily, both with clinically validated roles as anticancer drug targets. We report the discovery of the first class of dual inhibitors targeting the ATP-binding site of TopoIIα and the C-terminal domain of Hsp90, displaying potent cancer growth inhibition both *in vitro* and *in vivo*. Initially, a known TopoIIα inhibitor, compound **3**, was shown to bind to the C-terminal domain of Hsp90, but not to its ATP-binding N-terminal domain. Nineteen analogs were then prepared and evaluated to investigate the structure–activity relationships, several of which inhibited the growth of SK-N-MC Ewing sarcoma cells *in vitro*. Compound **3** emerged as one of the most potent growth inhibitors ($IC_{50} = 0.33 \pm 0.04$ μM), demonstrating the ability to induce apoptosis and cell cycle arrest in SK-N-MC cells *in vitro*, and to slow the growth of Ewing sarcoma *in vivo* in a zebrafish model.

1. Introduction

In 2021, cancer was the leading cause of death for people under the age of 65 in Europe, while in 2022, almost 10 million people across the world lost their battle against this disease [1,2]. To prevent this number from rising any further, the demand for new cancer therapies is high. One of the approaches that has become a cornerstone of oncology is combination therapy [3]. A vast proteome involved in cancer pathology enables combination therapies that exploit two or more different cancer-relevant targets to achieve a synergistic effect [4]. If the proteins in question are highly similar, a single molecule can be used to inhibit multiple targets, as is the case with multitarget kinase inhibitors [5,6].

The GHKL (**G**yrase, **H**sp90, Histidine **K**inase, Mut**L**) ATPase superfamily of proteins features a unique ATP-binding site. This site features a distinct Bergerat fold, which distinguishes it from other ATP-binding proteins, such as protein kinases [7]. Of the GHKL superfamily, the subfamilies of Hsp90 and topoisomerase II (TopoII) are cancer-relevant target proteins [8,9]. Apart from their similarities in the N-terminal domain ATP-binding sites, these proteins are quite distinct, and their functions are unrelated. Hsp90 is a family of four chaperones (Hsp90α, Hsp90β, Grp94, and TRAP-1), consisting of the ATP-binding N-terminal domain (NTD), the client protein-binding middle domain, and a C-

Abbreviations: 17-DMAG, 17-dimethylaminoethylamino-17-demethoxygeldanamycin; AMP-PCP, [[(2*R*,3*S*,4*R*,5*R*)-5-(6-aminopurin-9-yl)-3,4-dihydroxyoxolan-2-yl]methoxy-hydroxyphosphoryl]oxy-[[hydroxy(oxido)phosphoryl]methyl]phosphinate; CTD, C-terminal domain; DCM, dichloromethane; DMF, *N*,*N*-dimethylformamide; DSS, sodium trimethylsilylpropanesulfonate; EDC, 1-ethyl-3-(3-dimethylaminopropyl)carbodiimide; FTSA, fluorescence-based thermal shift assay; GHKL, Gyrase, Hsp90, Histidine Kinase, MutL; GST, glutathione S-transferase; HOBt, 1-hydroxybenzotriazole; Hsp, heat shock protein; Hsp90, heat shock protein 90; HSR, heat shock response; MD, molecular dynamics; MTS, 3-(4,5-dimethylthiazol-2-yl)-5-(3-carboxymethoxyphenyl)-2-(4-sulfophenyl)-2*H*-tetrazolium; NMM, *N*-methylmorpholine; NTD, N-terminal domain; SAR, structure–activity relationship; STD, saturation transfer difference; TBTU, 2-(1*H*-benzotriazole-1-yl)-1,1,3,3-tetramethylaminium tetrafluoroborate; TFA, trifluoroacetic acid; THF, tetrahydrofuran; TopoIIα, topoisomerase IIα; TR-FRET, time-resolved Förster's Resonance Energy Transfer; trNOESY, transferred nuclear Overhauser effect spectroscopy.

* Corresponding authors.
E-mail addresses: nace.zidar@ffa.uni-lj.si (N. Zidar), tihomir.tomasic@ffa.uni-lj.si (T. Tomašič).

https://doi.org/10.1016/j.bioorg.2024.107850
Received 1 August 2024; Received in revised form 19 September 2024; Accepted 26 September 2024
Available online 1 October 2024

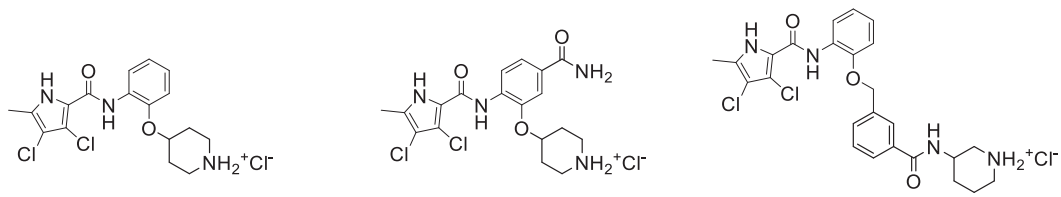

1
IC_{50} (TopoIIα) = 29 ± 19 μM
K_d (Hsp90α NTD) ≥ 200 μM
K_d (Hsp90β NTD) = 87 CI:[45;170] μM
IC_{50} (MCF-7) = 3.5 ± 0.8 μM

2
IC_{50} (TopoIIα) = 7.6 ± 0.4 μM
K_d (Hsp90α NTD) ≥ 200 μM
K_d (Hsp90β NTD) = 16 CI: [11;24] μM
IC_{50} (MCF-7) = 22 ± 10 μM

3
IC_{50} (TopoIIα) = 7.7 ± 3.6 μM
K_d (Hsp90α NTD) ≥ 200 μM
K_d (Hsp90β NTD) ≥ 200 μM
IC_{50} (MCF-7) = 0.15 ± 0.01 μM

Fig. 1. Structures of pyrrolamide-based dual TopoIIα and Hsp90β N-terminal domain inhibitors **1** and **2**, and newly discovered dual TopoIIα and Hsp90 C-terminal domain inhibitor **3** [26].

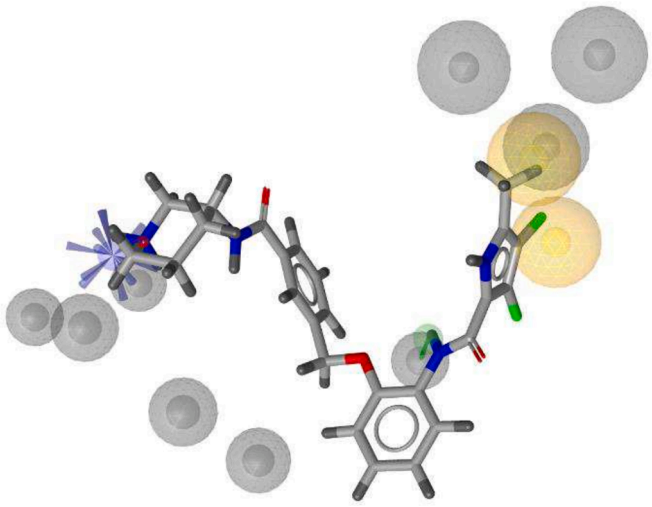

Fig. 2. Overlay of compound **3** with the structure-based pharmacophore model derived from the most representative molecular dynamics binding mode of inhibitor in the C-terminal domain binding site of the Hsp90β dimer [28] (PDB entry: 5FWK). Blue star represents a positively ionizable pharmacophore feature, green arrow a hydrogen bond donor pharmacophore feature, yellow spheres hydrophobic pharmacophore feature and grey spheres represent excluded volumes.

terminal domain (CTD) that is responsible for dimerization [10]. While Hsp90 expression is upregulated in numerous cancers, its contribution to disease progression is primarily driven by its influence on oncogenic client proteins, which depend on the Hsp90 family to preserve their active conformations [9,11]. Human TopoII is a subfamily of enzymes responsible for modulating the topology of double-stranded DNA [12]. The subfamily comprises two isoforms: TopoIIα, which is predominantly found in proliferating cells, including cancer cells, and TopoIIβ, which exerts its functions in all human cells. Like Hsp90, TopoII contains the NTD with the ATP-binding site, the catalytic site of the enzyme, which is located in the central domain, and the CTD, which is important for translocation of the enzyme into the nucleus [12,13].

Known anticancer drugs such as doxorubicin inhibit TopoIIα by intercalating between DNA base pairs, while the N-terminal binding site of TopoIIα enables for the development of ATP-competitive inhibitors [14,15]. Hsp90, on the other hand, was not a clinically validated target until 2022, when Hsp90α/β NTD inhibitor pimitespib was approved in Japan for the treatment of gastrointestinal stromal tumors [16]. Now, both proteins are clinically validated cancer targets and have overlapping ATP-binding sites in their respective NTDs [17]. Taken together, it is not surprising that dual inhibitors of the N-terminal binding sites of Hsp90 and TopoIIα have been described [17–19]. In addition, dual inhibitors of Hsp90 and other oncoproteins, such as histone deacetylase 6, tubulin and protein kinases, were recently reported [20].

Many ATP-competitive Hsp90 NTD inhibitors have been clinically investigated to date, but the development of most of them has been hampered by inefficacy and toxicity [9,11,21,22]. One of the biggest problems with these compounds has been the induction of the so-called heat shock response (HSR). In HSR, the heat shock proteins like Hsp70 and Hsp27 are overexpressed, which can abolish the inhibitory effect, leading to therapy ineffectiveness [23]. Fortunately, this response does not occur with inhibitors that target the CTD of Hsp90 [21,22,24]. Therefore, we hypothesized that this allosteric binding site on the Hsp90 CTD could be exploited for the design of dual inhibitors targeting both Hsp90 CTD and TopoIIα, thus circumventing the most notable disadvantages of N-terminal Hsp90 inhibition and displaying the synergistic anticancer activity by inhibiting two target proteins. Based on this initial assumption, our efforts resulted in the discovery of the first dual inhibitors of Hsp90 CTD and TopoIIα, which are described herein.

2. Results and discussion

2.1. Identification of dual TopoIIα and Hsp90 CTD inhibitors and design of analogs

Our in-house library of ATP-competitive pyrrolamide-based TopoIIα inhibitors was selected as a starting point for this study [25,26] as some of the compounds in this library, such as **1** and **2**, were shown to bind the NTD of Hsp90 (Fig. 1) [27]. We noticed, that by introducing a benzyl linker in compound **3**, the distance between the basic center and chloro-substituted aromatic moiety appears to be more similar to that in our previously published Hsp90 CTD inhibitors [28–33] than to known N-terminal inhibitors of Hsp90 [34,35]. To confirm this assumption, compound **3** was screened against our structure-based pharmacophore model for identification of Hsp90 CTD inhibitors [28]. Compound **3** matched the basic center (blue star), hydrogen bond donor (green arrow) and two hydrophobic pharmacophore features and thus contains all structural elements required for binding to Hsp90 CTD (Fig. 2).

First, using a fluorescence-based thermal shift assay (FTSA), the binding of compound **3** to the Hsp90α and Hsp90β NTD at concentrations up to 200 μM was investigated (Fig. 1 and Fig. S3). While compounds **1** and **2** bind to Hsp90β NTD in the micromolar range (Fig. 1), compound **3** showed no binding. Although all three compounds are structurally related, the introduction of a benzyl linker between the phenyl ring and piperidine in compound **3** appears to be detrimental for binding to the NTD of Hsp90. On the other hand, the introduction of this benzyl group has a positive effect on binding to TopoIIα, as compound **3** is at least a 3-fold more potent TopoIIα inhibitor than its analog **1**. However, despite equipotent TopoIIα inhibition by compounds **2** and **3**, the latter showed nearly 150-fold more potent antiproliferative activity in MCF-7 breast cancer cell line (Fig. 1). All these facts strengthened our

Table 1
Topoisomerase IIα inhibition, binding to Hsp90β C-terminal domain and antiproliferative activity in the Ewing sarcoma cell line SK-N-MC (mean ± SD) by the known topoisomerase IIα inhibitors **3**–**5** and newly prepared compounds **21**–**32**, **38**, **39** and **47**–**49**.

No.	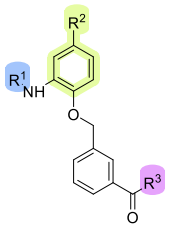			% of active TopoIIα at 10 μM and 100 μM		% of active Hsp90β CTD at 100 μM	SK-N-MC IC_{50} (μM)****
	R^1	R^2	R^3	10 μM	100 μM	100 μM	
3	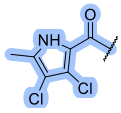		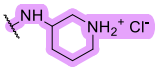	49.9	7.6	45.0	0.33 ± 0.04
4	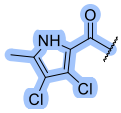		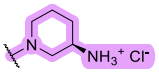	97.1	51.3	47.1	1.09 ± 0.06
5	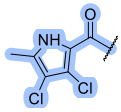		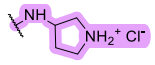	4.1	4.2	42.8	1.09 ± 0.02
21	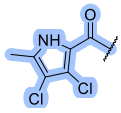		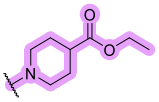	100	100	46.6	1.23 ± 0.03
22	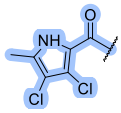		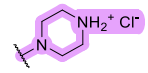	100	29.2	52.0	3.05 ± 0.07
23	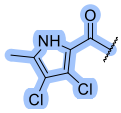		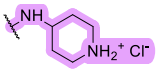	6.7	5.1	51.3	1.12 ± 0.06
24	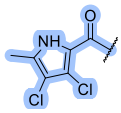		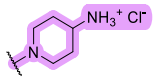	99.2	14.3	55.1	2.35 ± 0.08
25	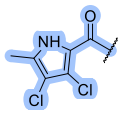		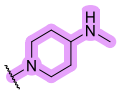	100	37.2	57.6	2.62 ± 0.26
26	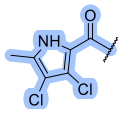		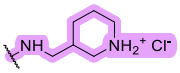	14.7	4.1	75.6	1.03 ± 0.08
27	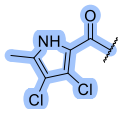		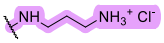	10.0	4.5	96.5	25.9 ± 7.7
28	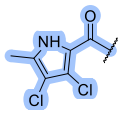		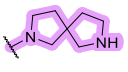	93.9	55.3	45.1	2.66 ± 0.00

(*continued on next page*)

Table 1 (*continued*)

No.	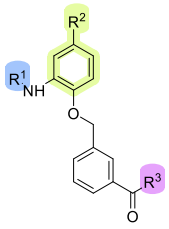			% of active TopoIIα at 10 μM and 100 μM		% of active Hsp90β CTD at 100 μM	SK-N-MC IC_{50} (μM)****
	R^1	R^2	R^3	10 μM	100 μM	100 μM	
29	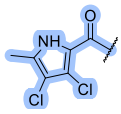		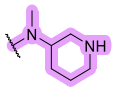	93.5	69.2	47.6	1.73 ± 0.53
30	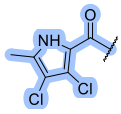		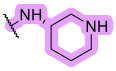	71.2	8.6	63.7	0.35 ± 0.05
31	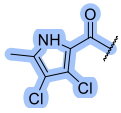		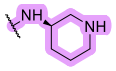	61.8	4.3	54.9	0.32 ± 0.05
32	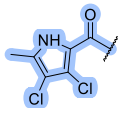		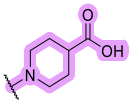	100**	100**	35.2	>50
38	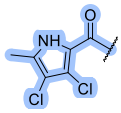		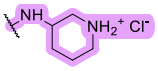	75.9	23.2	48.0	0.28 ± 0.01
39	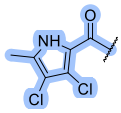		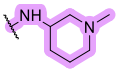	92.3	4.7	77.1	1.00 ± 0.08
47	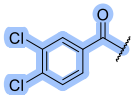		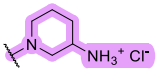	97.7	94.0	53.5	9.07 ± 2.79
48	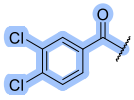		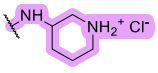	93.2	74.2	57.9	5.29 ± 1.27
49	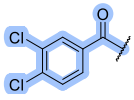		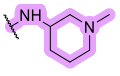	100	100	77.5	7.28 ± 1.82
	Etoposide				IC_{50} = 88.4 μM	n.t.*	n.t.*
	Novobiocin			n.t.*	n.t.*	34.3***	171 ± 7

n.t.* – not tested; ** – 10 and 50 μM concentrations of **32** in EtOH/NaOH mixture were used due to poor solubility; *** – novobiocin was tested at 1000 μM as the positive control; **** IC_{50} values are reported as mean ± SD of duplicates.

belief that compound **3** binds to an additional cancer-relevant target and that the proposed C-terminal Hsp90 inhibition may be the cause of this spike in antiproliferative activity.

We first examined the binding of compound **3** to the C-terminal domain of Hsp90 using a TR-FRET-based assay. In this assay, inhibitors of the Hsp90 CTD prevent the interaction between Hsp90β CTD and PPID [24,36], causing the distance between donor beads (bound to PPID *via* a GST-tag) and acceptor beads (bound to Hsp90 *via* biotin) to increase. This elongation prevents the light emitted by the donor beads from reaching the acceptor beads. Compound **3** inhibited 55 % of the interaction of Hsp90β CTD and its cochaperone cyclophilin D (PPID) at 100 μM. This confirms that compound **3** is a dual inhibitor of TopoIIα and Hsp90β CTD. Similarly, binding to Hsp90 CTD was confirmed for TopoIIα inhibitors **4** and **5** (Table 1), the two known analogs of compound **3** [26]. To better understand the key structural features of the dual mode of action, we investigated the most likely binding mode of

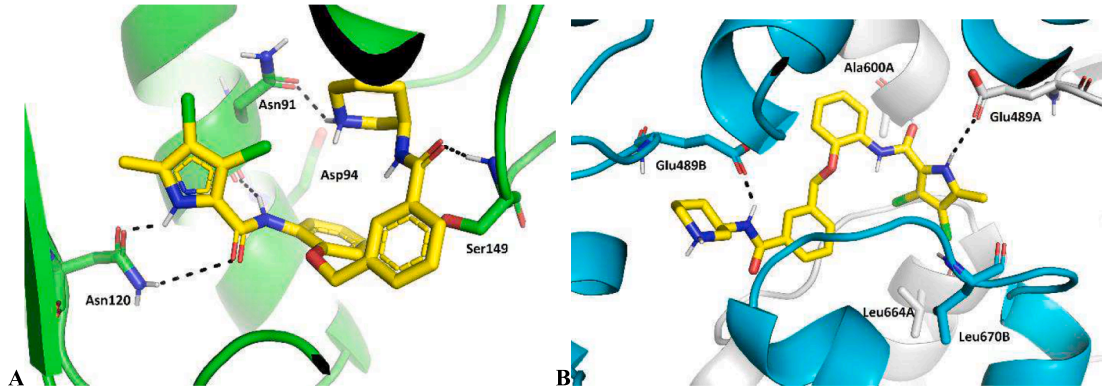

Fig. 3. Predicted binding mode of (*R*)-**3** (in yellow sticks) in the **(a)** ATP-binding site of the human topoisomerase IIα (PDB entry: 4R1F, in green cartoon), and **(b)** allosteric binding site at the Hsp90β C-terminal domain (PDB entry: 5FWK, protomer A in grey cartoon, protomer B in cyan cartoon). Hydrogen bonds between the protein and (*R*)-**3** are presented as black dashed lines.

compound **3** to TopoIIα (PDB entry: 4R1F) [37] and Hsp90β CTD (PDB entry 5FWK) [38] using a combination of molecular docking, molecular dynamics simulations, and protein–ligand interaction analysis. Since compound **3** is a racemic mixture, both enantiomers were docked in the ATP-binding site of the human TopoIIα and Hsp90β CTD binding site. Docking calculations revealed that in both proteins, the (*R*)-enantiomer of compound **3** had slightly higher scoring function scores. In the case of TopoIIα (Fig. 3A), the pyrrolamide moiety forms two hydrogen bonds with the Asn120 side chain, while the basic center of the piperidine ring forms a hydrogen bond with Asn91 and an ionic interaction with Asp94. These interactions are well preserved during the 200 ns MD simulation (Fig. S1). The inhibitor is further stabilized in the binding site by a hydrogen bond with Ser149 and a network of hydrophobic contacts. During the MD trajectory, additional hydrogen bonds with Arg98 and Ser148 are predicted (Fig. S1). In the Hsp90β CTD binding site (Fig. 3B), the pyrrole NH forms a hydrogen bond with the Glu489A side chain,

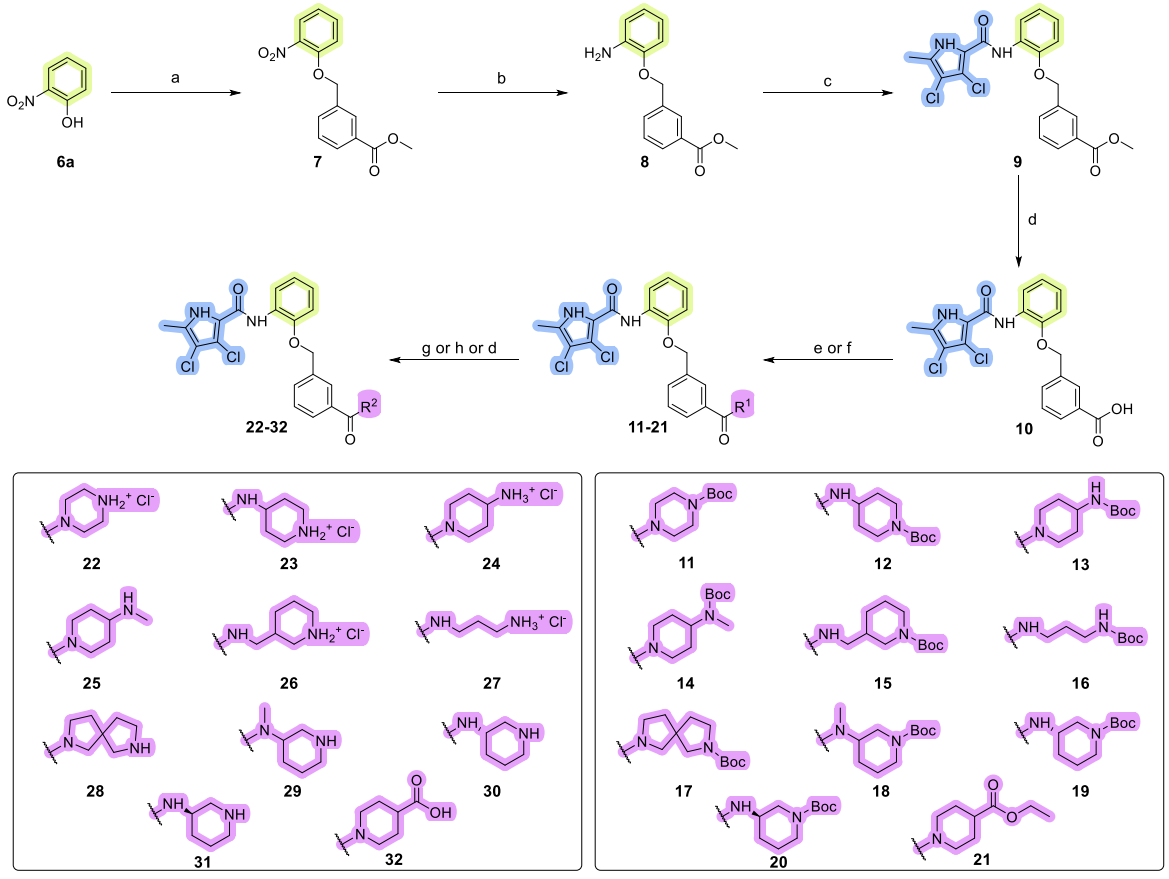

Scheme 1. *Reagents and conditions.* (a) methyl 3-(bromomethyl)benzoate, K_2CO_3, MeCN, 60 °C, overnight, yield: 90 %; (b) $Fe_{(s)}$, CH_3COOH, 60 °C, overnight, yield: 49 %; (c) i) 3,4-dichloro-5-methyl-1*H*-pyrrole-2-carboxylic acid, $SOCl_2$, 70 °C, 1 h; ii) pyridine, DCM, r.t., overnight, yield: 86 %; (d) for the synthesis of **10** and **32**: 2 M $NaOH_{(aq)}$, MeOH:THF = 1:2, 60 °C, overnight, yield: 93–95 %; (e) for the synthesis of **11**–**13**, **15**, **16**: i) TBTU, NMM, DMF, r.t., 15 min; ii) corresponding amine, r.t., overnight, yield: 49–81 %; (f) for the synthesis of **14**, **17**–**21**: i) EDC, HOBt, NMM, DMF, 0 °C, 20 min; ii) corresponding amine, r.t., overnight, yield: 54–90 %; (g) for the synthesis of **22**–**24**, **26**–**27**: 4 M HCl in 1,4-dioxane, DMF, r.t., overnight, yield: 31–98 %; (h) for the synthesis of **25**, **28**–**31**: TFA, DCM, r.t., overnight, yield: 43–80 %.

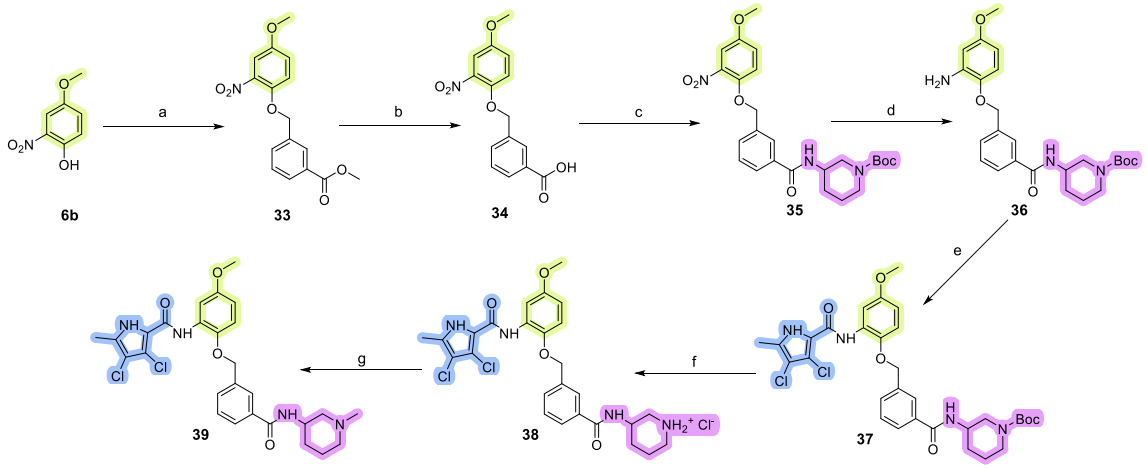

Scheme 2. *Reagents and conditions.* (a) methyl 3-(bromomethyl)benzoate, K_2CO_3, MeCN, 60 °C, overnight yield: 62 %; (b) 2 M $NaOH_{(aq)}$, MeOH:THF = 1:2, 60 °C, overnight, yield: 96 %; (c) i) TBTU, NMM, DMF, r.t., 15 min; ii) *tert*-butyl 3-aminopiperidine-1-carboxylate, r.t., overnight, yield: 94 %; (d) $Fe_{(s)}$, CH_3COOH, 60 °C, overnight, yield: 39 %; (e) i) 3,4-dichloro-5-methyl-1*H*-pyrrole-2-carboxylic acid, $SOCl_2$, 70 °C, 1 h; ii) pyridine, DCM, r.t., overnight, yield: 42 %; (f) 4 M HCl in 1,4-dioxane, DMF, r.t., overnight, yield: 84 %; (g) i) 37 % formaldehyde$_{(aq)}$, Et_3N, MeOH, r.t., 60 min; ii) $NaCNBH_3$, r.t., overnight, yield: 65 %.

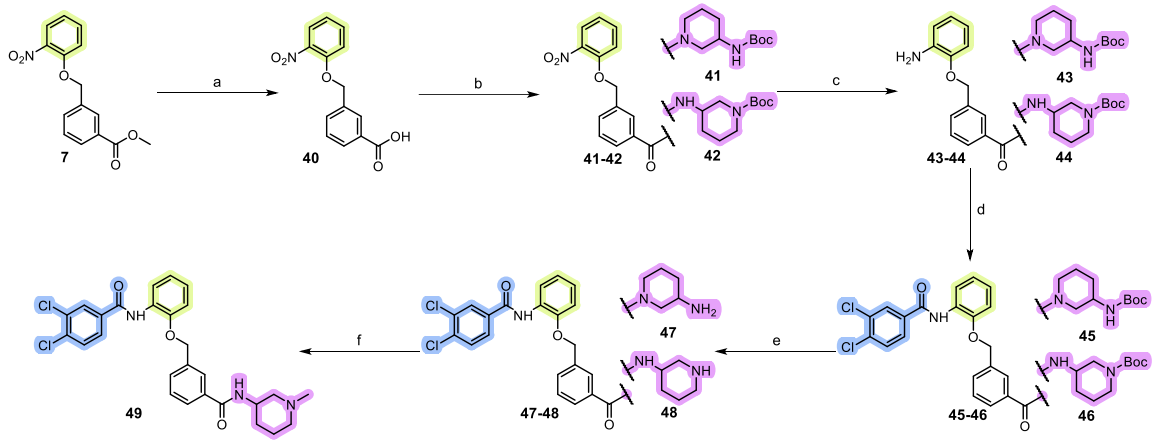

Scheme 3. *Reagents and conditions.* (a) 2 M $NaOH_{(aq)}$, MeOH:THF = 1:2, 60 °C, overnight, yield: 81 %; (b) i) EDC, HOBt, NMM, DMF, 0 °C, 20 min; ii) corresponding amine, r.t., overnight, yield: 79–97 %; (c) $Fe_{(s)}$, CH_3COOH, 60 °C, overnight, yield: 64–90 %; (d) i) 3,4-dichlorobenzoic acid, EDC, HOBt, NMM, DMF, 0 °C, 20 min; ii) corresponding amine, r.t., overnight, yield: 34–49 %; (e) TFA, DCM, r.t., overnight, yield: 68–78 %; (f) i) 37 % formaldehyde$_{(aq)}$, Et_3N, MeOH, r.t., 60 min; ii) $NaCNBH_3$, r.t., overnight, yield: 75 %.

present in 26 % of the simulation time, suggesting it is not critically important for binding (Fig. S2). However, the carbonyl group at position 2 forms a hydrogen bond with Leu670B for 63 % of the simulation time. An additional hydrogen bond is formed between the Glu489B side chain and the amide bond of (*R*)-**3** in the docking complex (Fig. 3B), which is mostly a water-mediated interaction in the MD simulation trajectory (Fig. S2). Additional hydrogen bonds with Arg604A and Ser669A, as well as an ionic interaction with the Glu603A side chain, are also predicted (Fig. S2).

2.2. Synthesis

A focused library of new analogs was then designed and synthesized (Schemes 1–3) to study the structure–activity relationship (SAR). To do so, different heterocyclic amines were introduced in compounds **22**–**31** (Scheme 1). Based on the results of our previous studies [29,32], small variations in the distance between the halogen-substituted aromatic ring and basic center can have significant effects on Hsp90 CTD binding and antiproliferative activity. Carboxylic acid **32** (Scheme 1) and its ethyl ester **21** were prepared to study the importance of the basic amine on Hsp90 CTD and TopoIIα inhibition. Synthesis of these compounds started with the preparation of ether **7** by alkylation of the 2-nitrophenol with the methyl 3-(bromomethyl)benzoate in the presence of potassium carbonate as base. In the following step, the nitro group of **7** was reduced to amine **8**, which was then coupled with the 3,4-dichloro-5-methyl-1*H*-pyrrole-2-carboxylic acid to amide **9**. The latter was first hydrolyzed under basic conditions to carboxylic acid **10** that was used to synthesize amides **11**–**21**. To obtain final compounds **22**–**31**, acidolysis was employed to deprotect the Boc group of carbamates **11**–**20**, while compound **32** was prepared by basic hydrolysis of ester **21**.

To enrich the electron density of the phenyl ring bearing the pyrrolamide moiety, electron-donating methoxy group was introduced to study the potential of the methoxyphenyl moiety for formation of cation-π and π–π interactions. Methoxyphenyl analog of compound **3** was synthesized using an analogous synthetic methodology as described above (Scheme 2). Formation of ether **33** was followed by alkaline ester hydrolysis (compound **34**) and coupling to prepare amide **35**. Then, amine **36** was obtained by reduction of the nitro group in **35** and coupled with the substituted pyrrole-2-carboxylic acid to give amide **37**. Compound **38** was obtained by Boc-deprotection and in the final step the amine group was methylated under reductive amination conditions to obtain compound **39**.

Based on the binding mode studies and SARs of our previously developed Hsp90 CTD inhibitors, hydrogen bonding with Glu489A side

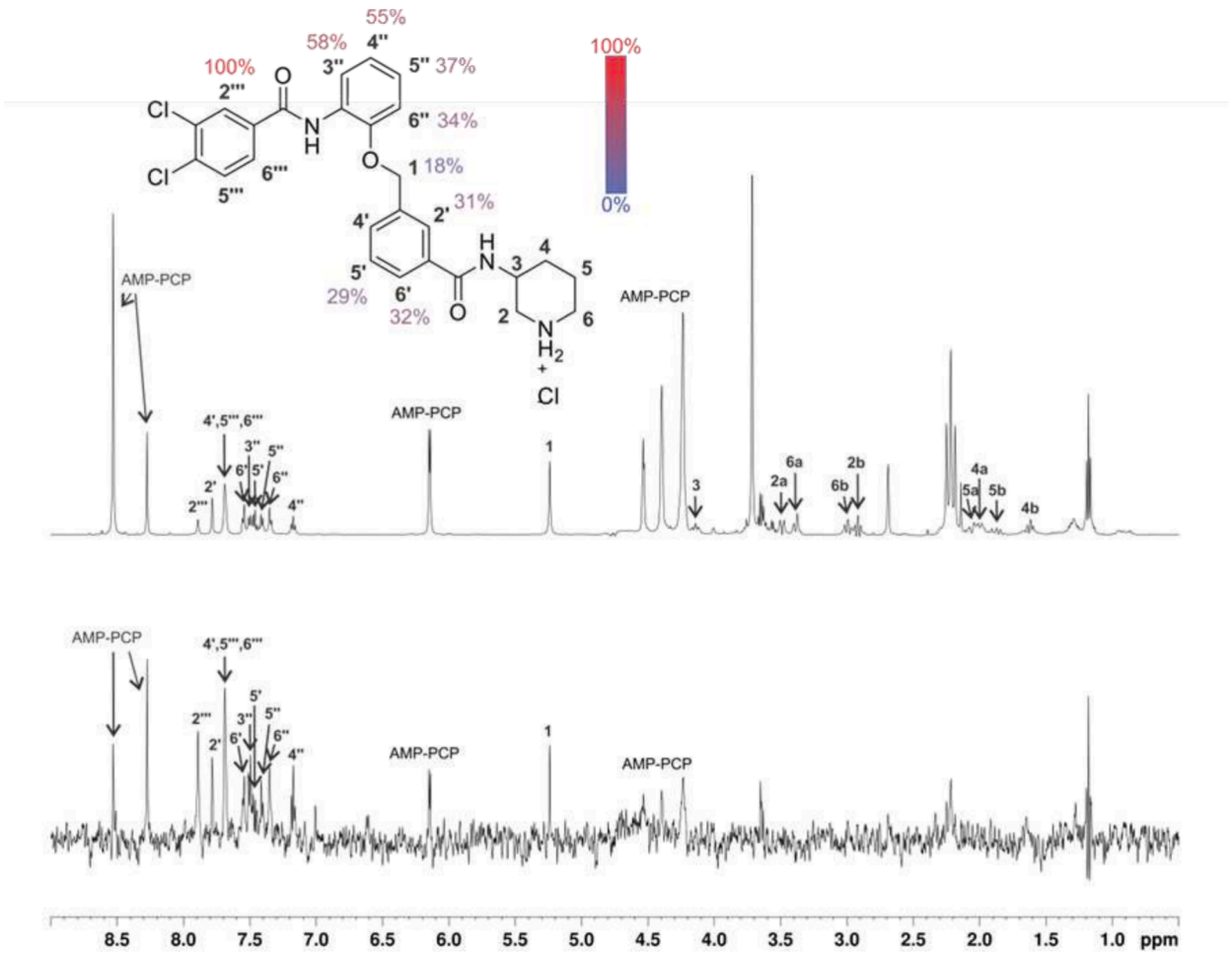

Fig. 4. 1D ^{1}H STD NMR spectra for the compound **48** recorded at a Hsp90β:ligand ratio of 1:100 and 600 MHz. The structure of **48** shows the proton nomenclature and the color-coded relative degrees of saturation of the individual not-overlapped protons. The STD amplification factors were normalized to the intensity of the signal with the largest STD effect. The reference STD spectrum (top) with proton assignment and the difference STD spectrum (bottom) are shown. The unassigned proton signals between 3.5 and 3.8 ppm belong to protein buffer with glycerol. Signal for 3 partially overlaps with signals of AMP-PCP and signal for 2a partially overlaps with signals of protein buffer with glycerol. Intensities of 2, 3, 4, 5 and 6 are under detection limit in the difference STD spectrum. Since signals for 4′, 5‴ and 6‴ are overlapped, their STD amplification factors could not be determined. The proton signals were calibrated to the DSS signal at 0.0 ppm. The spectra are not to scale.

chain is not critical for binding. In fact, in the binding pocket to which the 3,4-dichloro-5-methylpyrrolamide moiety of **3** binds, halogen-substituted phenyl rings such as 3,4-dichlorophenyl are very well tolerated [29,30,32]. On the other hand, according to the predicted binding mode of compound **3** in the ATP-binding site of TopoIIα (Fig. 3a), replacement of the substituted pyrrolamide moiety would most likely be detrimental for the inhibitory activity. To test this hypothesis, the 3,4-dichlorophenyl group-containing final compounds **47**–**49** were synthesized according to Scheme 3. After ester hydrolysis, the obtained compound **40** was coupled with Boc-protected 3-aminopiperidines to prepare amides **41** and **42**. Reduction of the nitro groups of the latter to amines **43** and **44** was followed by coupling with the 3,4-dichlorobenzoic acid to yield **45** and **46**. Acidolysis of **45** and **46** resulted in final amines **47** and **48**. Compound **48** was further methylated using formaldehyde and sodium cyanoborohydride to prepare tertiary amine **49**. All final compounds were then screened for their TopoIIα inhibition using a DNA relaxation assay (Fig. S4) and for their C-terminal Hsp90 inhibition using the TR-FRET-based assay.

2.3. Biological evaluation and structure–activity relationships

The results clearly indicate the importance of the 5-methyl-3,4-dichloropyrrole moiety (compounds **22**–**31**, **38** and **39** vs compounds **47**–**49**) and the basic center (compounds **22**–**31**, **38** and **39** vs compounds **21** and **32**) for TopoIIα inhibition, while compounds **47**–**49** showcase that the pyrrole moiety is not necessary for the binding to Hsp90 CTD. Additionally, the basic center appears to have a less important role in Hsp90 CTD inhibition of this compound series, as both neutral **21** and acidic **32** retain their ability to modulate Hsp90 activity, while the introduction of basic propylamine substituent in **27** results in an inactive compound considering only Hsp90 CTD inhibition. The SAR is consistent with the predicted binding poses for compound **3** in the TopoIIα and Hsp90 CTD binding sites (Fig. 3). Interestingly, compounds **30** and **31**, which are *S*- and *R*- enantiomers of compound **3**, displayed nearly equipotent activity against both target proteins. To better understand the binding mode of this compound class to the Hsp90β CTD, the binding contributions of the Hsp90-selective compound **48** were evaluated using STD NMR. Group epitope mapping analysis revealed that the binding is primarily mediated by the 3,4-dichlorobenzamide moiety (Fig. 4, Tables S1 and S2). Proton 2‴ showed the highest degree of saturation, indicating its closest proximity to Hsp90β. The STD amplification factors of other protons suggest that the phenoxy ring forms stronger contacts with the binding site compared to the benzamide moiety, which is linked to the piperidine ring. Consequently, the phenoxy ring likely contributes more significantly to the binding of compound **48** and similar analogs. In contrast, the aliphatic protons of

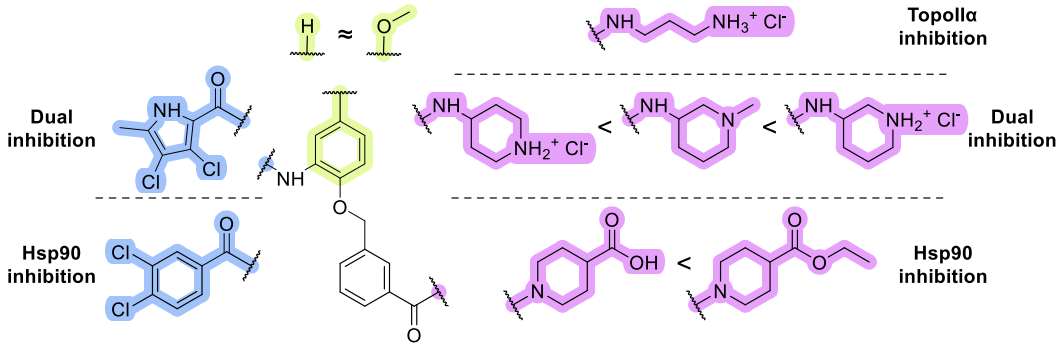

Fig. 5. Structure-activity relationship summary for on-target activity and antiproliferative activity in cancer cells. 3,4-Dichloro-5-methylpyrrolamide (in blue) moiety is critical for dual-target inhibition, while its replacement with the 3,4-dichlorobenzamide (in blue) moiety results in selective Hsp90 CTD inhibition. Introduction of the methoxy group on the adjacent phenyl ring (in yellow) results in equipotent activity, while modification of the nitrogen-based heterocycle (in magenta) results in the most pronounced effects on target inhibition and antiproliferative activity.

the oxymethylene and piperidine rings form the weakest contacts with the protein binding site. Additionally, the interaction of compound **48** with Hsp90β was further validated through trNOESY experiments, which revealed negative NOEs sharing the same sign as the diagonal peaks between the inhibitor's protons in the presence of Hsp90β. These NOEs were detected only between neighboring molecular regions, indicating that compound **48** assumes an extended conformation when bound to Hsp90β (Fig. S6).

Due to the promising inhibitory activities in target-based assays and confirmed dual mechanism of action of several inhibitors, all compounds were tested for their antiproliferative activity in the Ewing sarcoma cell line SK-N-MC using an MTS-based assay. Ewing sarcoma is one of the most common malignant bone and soft tissue tumors in children and adolescents. Despite effective treatment of localized Ewing sarcoma, long-term survival of patients with metastatic or relapsed disease remains very low [39]. Several oncoproteins of Ewing sarcoma are Hsp90 client proteins, but Hsp90 as a therapeutic option remains underexplored [40]. In addition, agents targeting topoisomerase II show potential when used as a combination therapy [41,42], making combined inhibition of TopoIIα and Hsp90 CTD an appealing new approach for Ewing sarcoma growth inhibition which was determined by an MTS-based assay. The results presented in Table 1 are given as concentrations at which the cell growth is inhibited by half (IC_{50} values) relative to the maximal growth of the negative control. The IC_{50} values highlight the advantages of dual TopoIIα and Hsp90 CTD inhibition, as the compounds with the most potent antiproliferative activity inhibit both proteins. This is consistent with previous reports, as compound **3** has outperformed other equipotent TopoIIα inhibitors in MCF-7 breast cancer cell line [26]. Moreover, our C-terminal Hsp90 inhibitors with similar inhibitory potential for Hsp90 displayed weaker potency in Ewing sarcoma cancer cells [32,43] compared to compounds **3**, **29**, **30** and **38**, which inhibit both the CTD of Hsp90 and the NTD of TopoIIα. Among the newly prepared compounds, Hsp90 CTD-selective inhibitors **47**–**49** and TopoII-selective inhibitor **27** show the weakest antiproliferative activities among the compounds tested. Interestingly, the ethyl ester **21** is a more potent growth inhibitor in Ewing sarcoma cells than **47**–**49**, although all compounds only inhibit the Hsp90 CTD. Meanwhile, its carboxylic acid analog **32** exhibits even stronger Hsp90 inhibition but is inactive in the cells. This potentially indicates the permeability issue in cell-based assay, as the uptake across the membrane is commonly problematic for carboxylic acids [44]. SAR for on-target and cellular activity is summarized in Fig. 5. In addition to dual-target inhibitors, we identified also Hsp90 CTD- and TopoIIα-selective compounds, which greatly impacts their antiproliferative activities. Overall, compound **3**, which remained the most potent growth inhibitor in the Ewing sarcoma cell line SK-N-MC, was selected for further investigation.

The induction of apoptosis is a well-established feature of both TopoIIα and Hsp90 inhibitors [45–49]. Compound **3** induced apoptosis in SK-N-MC cells after only 24 h of treatment (Fig. 6A). The effect at this time point at 1.5 μM and 7 μM of compound **3** was equipotent as the portion of apoptotic cells exceeded 90 % (Fig. S7). A similar effect was measured after 72 h at both concentrations indicating a persisting induction of apoptosis. The effect of 24-h treatment was less pronounced at the lowest concentration – 0.375 μM. Here combined fractions of early and late apoptotic cells amounted to 21.0 % compared to 16.5 % in the vehicle control (0.5 % DMSO). The effect of 0.375 μM of compound **3**, after 72 h of incubation was even less potent (7.2 % of apoptotic cells vs. 6.8 % in vehicle control). Overall, the data suggest that the induction of apoptosis was not time-dependent, whereas an increase from 0.375 μM concentration to 1.5 μM of compound **3** resulted in a significant spike in apoptosis (Fig. S7). Based on these data, the cells were treated with 0.70 μM and 1.5 μM of **3** for 24 and 48 h to complementary evaluate the effect on cell cycle progression in SK-N-MC cells (Fig. S8). No statistically significant arrest in any of the phases was observed. However, a trend for cell cycle arrest in G2/M phase was observed after 24 h, which is in line with previously reported data, showing that TopoIIα levels reach their peak after 24 h [45–47]. Meanwhile, after 48 h, most cells have accumulated in the G0/G1 cell cycle phase, as was previously reported for several N- and C-terminal inhibitors of Hsp90 along with their G2/M arrest induction potential [48–51]. Additionally, Western blot analysis (Fig. 6B) showed a notable decrease in the levels of a known Hsp90 client protein c-Raf [52] after 24 h of exposure to 1 μM and 5 μM concentration of compound **3**. Simultaneously, no significant induction of heat shock response was observed as the levels of Hsp70 and Hsp90 were not affected, again pointing to C-terminal inhibition of Hsp90 [21].

Finally, as compound **3** also displayed selectivity for Ewing sarcoma cells (selectivity index = 6.4) compared to human embryonic kidney-derived HEK293 cells (IC_{50} = 2.1 ± 0.6 μM [26]), it was progressed to *in vivo* testing in an Ewing sarcoma zebrafish xenograft model (Fig. 6C), which has been previously used for the evaluation of C-terminal Hsp90 inhibitors [53]. In this assay, a clinically evaluated Hsp90 inhibitor 17-DMAG was used as a positive control, while 1 % DMSO served as the negative control. As shown in Fig. 6D, compound **3** was more potent in inhibiting tumor growth than 17-DMAG, as it statistically significantly inhibited the growth of SK-N-MC-derived tumors at a concentration of 10 μM. In contrast, 17-DMAG inhibited tumor growth to a similar degree but was administered at a 3-fold higher concentration of 30 μM. No developmental defects of zebrafish larvae were observed at these concentrations. From these data, it can be concluded that dual inhibitors of TopoIIα and Hsp90 CTD not only inhibit cancer cell growth *in vitro*, but also show greater efficacy in an *in vivo* model compared to a clinically evaluated Hsp90 NTD inhibitor.

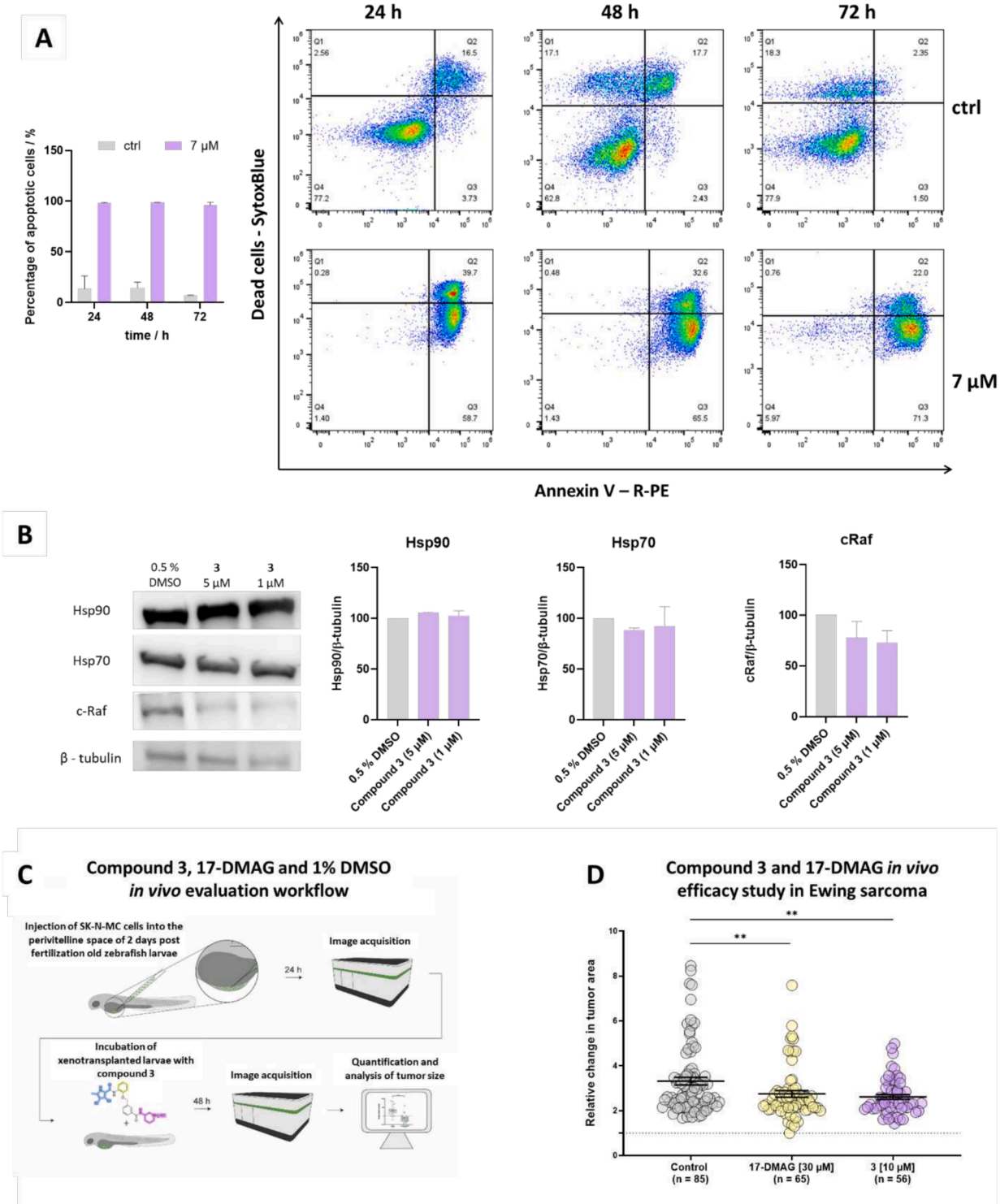

Fig. 6. Insights into the cytostatic and cytotoxic behavior of compound **3**. **(A)** Time dependency of apoptosis with corresponding representative experiments measuring the changes in proportion of Annexin V and/or SytoxBlue positive SK-N-MC cells (right). The bar graph represents means and SD of at least two independent experiments (left). **(B)** Effect of compound **3** on Hsp90 client protein c-Raf and heat shock proteins Hsp70 and Hsp90 in Ewing sarcoma cell line SK-N-MC after 24 h of treatment. Full images used for quantification are shown in Supporting information Fig. S9. **(C)** Schematic representation of the workflow applied for the *in vivo* evaluation of compound **3** and 17-DMAG in zebrafish larvae xenograft model of Ewing sarcoma. **(D)** Graphical depiction of a statistically significant inhibition of increase in relative change in tumor size in larvae treated with 1 % DMSO vs. 17-DMAG (30 µM) vs. compound **3** (10 µM); Error bars represent mean ± SEM. Statistical analysis was performed with a Mann Whitney test (**$p < 0.01$).

3. Conclusion

Using known TopoIIα inhibitors and our previously described *in silico* approaches for designing C-terminal Hsp90 inhibitors, we discovered the first series of compounds that bind to both the CTD of Hsp90 and TopoIIα. The synergistic potential of dual-mode action was confirmed, as the most potent TopoIIα and C-terminal Hsp90 inhibitors were also the strongest *in vitro* anticancer agents, achieving high nanomolar IC_{50} values in the Ewing sarcoma cancer cell line SK-N-MC. Among the most potent compounds, dual inhibitor **3** was further shown to affect Hsp90 client protein c-Raf levels without HSR induction, induce apoptosis and cause cell cycle arrest in Ewing sarcoma cells *in vitro*, leading to a statistically significant tumor growth reduction *in vivo* in a zebrafish larvae xenograft model of SK-N-MC cells. These findings suggest that the dual inhibitors of Hsp90 CTD and TopoIIα represent a promising new modality in cancer treatment. The most potent compounds identified in this study are promising candidates for further development and preclinical evaluation.

4. Materials and methods

4.1. Chemistry

The solvents and reagents employed in the synthesis of final products and intermediates were obtained from various suppliers, including Sigma-Aldrich based in St. Louis, MO, USA, Enamine Ltd. based in Kyiv, Ukraine, Tokyo Chemical Industry Co., Ltd. nased in Tokyo, Japan, Apollo Scientific Ltd. based in Stockport, UK, and Fluorochem Ltd. based in Derbyshire, UK. All reagents were used as received without further purification. Analytical TLC (thin-layer chromatography) was performed using silica gel aluminum sheets (0.20 mm; 60 F254) acquired form Merck, based in Darmstadt, Germany. Meanwhile, for column chromatography silica gel 60 (particle size, 230–400 mesh) was utilized as the stationary phase. Chemical compounds were analyzed using a 400 MHz NMR spectrometer (Bruker Advance 3, Bruker, Billerica, MA, USA) for recording ^{1}H- and ^{13}C NMR spectra. The splitting patterns were designated as follows: s, singlet; br s, broad singlet, d, doublet; t, triplet; dt, double triplet; q, quartet; p, pentet; and m, multiplet. Ultra-high performance liquid chromatography (UHPLC, Thermo Scientific Dionex UltiMate 3000 UHPLC modular system, produced by Thermo Fisher Scientific Inc., Waltham, MA, USA) was used to monitor the purity of the final compounds. The UHPLC was equipped with a wavelength detector set to 254 nm for purity determination. The purity determination method used a C18 column (Waters Acquity UHPLC® HSS C18 SB column, 2.1 mm × 50 mm, 1.8 μm) with the oven temperature set to 40 °C. Sample injection volume was 5 μL, and the mobile phase flow rate was 0.3 mL/min, consisting of appropriate ratios of Solvent A (0.1 % TFA in H_2O) and Solvent B (CH_3CN). In the elution gradient was first from 0 → 7 min 5 % B was applied, which was increased to 95 % B from 7 → 8 min. Mass spectra were recorded using an Expression CMSL mass spectrometer (Advion Inc., Ithaca, NY, USA), and high-resolution mass spectra were obtained with an Exactive Plus Orbitrap mass spectrometer (Thermo Scientific Inc., Waltham, MA, USA). The purity of all final compounds was confirmed to be greater than 95 %.

4.1.1. General procedure A

The corresponding phenol (1.1 equiv.) and K_2CO_3 (2 equiv.) were taken up in acetonitrile and methyl 3-(bromomethyl)benzoate (1 equiv.) was added. Then the reaction mixture was stirred overnight at 60 °C. The volatiles were evaporated under reduced pressure and the residue was taken up in ethyl acetate (100 mL) and water (60 mL). The phases were separated, and the organic layer was additionally washed with 1 M $NaOH_{(aq)}$ (3 × 50 mL) and brine (2 × 40 mL). The organic layer was dried over Na_2SO_4, filtered, and the volatiles were evaporated under reduced pressure.

4.1.2. General procedure B

The corresponding substituted nitrobenzene (1 equiv.) was dissolved in acetic acid (20 mL) and solid iron (10 equiv.) was added. The reaction mixture was stirred overnight at 60 °C. The mixture was diluted with water (10 mL) and methanol (10 mL) and filtered over Celite® 545. The solvent of the mother liquor was evaporated under reduced pressure. The residue was taken up in EtOAc (50 mL) and washed with $NaHCO_3$ (45 mL) and NaCl (20 mL) and dried over Na_2SO_4. The solvent was then evaporated under reduced pressure.

4.1.3. General procedure C

3,4-Dichloro-5-methyl-1H-pyrrole-2-carboxylic acid (1.2 equiv.) was dissolved in $SOCl_2$ (2 mL/mmol), the reaction mixture was heated to 70 °C for 1 h and the volatiles were evaporated under reduced pressure to yield an acid chloride. Corresponding aromatic amine (1 equiv.) was dissolved in anhydrous DCM (10 mL/mmol) and pyridine (1 mL/mmol) under an argon atmosphere. The prepared mixture was added to previously prepared acid chloride and the reaction mixture was stirred under an argon atmosphere at room temperature overnight. The volatiles were evaporated under reduced pressure.

4.1.4. General procedure D

Corresponding methyl ester (1 equiv.) was taken up in a mixture of MeOH and THF (1:2 respectively). Then 2 M $NaOH_{(aq)}$ (5 equiv.) was added to the solution and the reaction mixture was stirred overnight at 60 °C. The solvent was evaporated, and water was added to the residue. The solution was acidified to pH = 1 and the formed precipitate was filtered off, washed with Et_2O and dried.

4.1.5. General procedure E

Respective carboxylic acids (1 equiv.) were dissolved in DMF. 2-(1*H*-Benzotriazole-1-yl)-1,1,3,3-tetramethylaminium tetrafluoroborate (TBTU, 1.3 equiv.), and *N*-methylmorpholine (NMM, 2 equiv.) were added at room temperature and the reaction mixture was stirred for 15 min. The corresponding amine was added, and the mixture was stirred overnight at room temperature. Afterwards, the volatiles were evaporated under reduced pressure and the residue was taken up in EtOAc, which was then washed with 1 M $HCl_{(aq)}$ (2 × 25 mL) and saturated $NaHCO_{3(aq)}$ (2 × 25 mL). The organic layer was washed with brine (50 mL), dried over Na_2SO_4, filtered, and the volatiles were evaporated under reduced pressure.

4.1.6. General procedure F

Respective carboxylic acids (1 equiv.) were dissolved in DMF. 1-Ethyl-3-(3-dimethylaminopropyl)carbodiimide (EDC, 1.2 equiv.), 1-hydroxybenzotriazole (HOBt, 1.3 equiv.) and *N*-methylmorpholine (NMM, 2 equiv.) were added at 0 °C. The reaction mixture was stirred for 20 min and then the corresponding amine was added, and the mixture was stirred overnight at room temperature. Afterwards, the volatiles were evaporated under reduced pressure and the residue was taken up in EtOAc, which was then washed with 1 % citric acid (2 × 50 mL) and $NaHCO_{3(aq)}$ (2 × 50 mL). The organic layer was washed with brine (50 mL), dried over Na_2SO_4, filtered, and the volatiles were evaporated under reduced pressure. When necessary, the product was further purified by flash column chromatography using a suitable ratio of DCM to MeOH as the eluent.

4.1.7. General procedure G

The corresponding Boc-protected amine (0.25 mmol) was dissolved in DMF (4 mL) and 4 M HCl in 1,4-dioxane (4 mL) was added. The mixture was stirred overnight at room temperature. The volatiles were evaporated under reduced pressure. The residue was then suspended in acetonitrile and the precipitate was collected and dried.

4.1.8. General procedure H

The corresponding Boc-protected amine (1 equiv.) was dissolved in

DCM (5 mL/0.1 mmol) and then trifluoroacetic acid (20 equiv.) was added. Next, the reaction mixture was stirred at room temperature overnight and then the volatiles were evaporated under reduced pressure.

4.1.9. Methyl 3-((2-nitrophenoxy)methyl)benzoate (7) [26]

The synthesis was performed in accordance with general procedure A using 2-nitrophenol (4.00 g, 28.8 mmol) as starting material. Yield: 90 % (6.73 g); yellow amorphous solid; ^{1}H NMR (400 MHz, DMSO-d_6) δ 8.09 (s, 1H), 7.92 (ddd, 2H, $J_1 = 11.4$ Hz, $J_2 = 8.0$ Hz, $J_3 = 1.5$ Hz), 7.74 (d, 1H, $J = 8.1$ Hz), 7.67 (ddd, 1H, $J_1 = 8.6$ Hz, $J_2 = 7.4$ Hz, $J_3 = 1.7$ Hz), 7.58 (t, 1H, $J = 7.7$ Hz), 7.46 (dd, 1H, $J_1 = 8.5$ Hz, $J_2 = 0.9$ Hz), 7.19 – 7.11 (m, 1H), 5.41 (s, 2H), 3.87 (s, 3H) ppm; ^{13}C NMR (101 MHz, DMSO-d_6) δ 166.0, 150.7, 139.7, 136.8, 134.5, 132.0, 129.9, 129.0, 128.8, 128.0, 125.1, 120.9, 115.5, 69.8, 52.2 ppm; MS (ESI+) m/z = 310.1 $[M+Na]^+$.

4.1.10. Methyl 3-((2-aminophenoxy)methyl)benzoate (8) [26]

The synthesis was performed in accordance with general procedure B using compound **7** (6.65 g, 23.2 mmol) as starting material. Yield: 49 % (2.94 g); light red amorphous solid; ^{1}H NMR (400 MHz, DMSO-d_6) δ 8.05 (t, 1H, $J = 1.8$ Hz), 7.92 (dt, 1H, $J_1 = 7.8$ Hz, $J_2 = 1.5$ Hz), 7.80 (dt, 1H, $J_1 = 8.0$ Hz, $J_2 = 1.3$ Hz), 7.56 (t, 1H, $J = 7.7$ Hz), 6.86 (dd, 1H, $J_1 = 7.9$ Hz, $J_2 = 1.2$ Hz), 6.73–6.64 (m, 2H), 6.49 (ddd, 1H, $J_1 = 7.9$ Hz, $J_2 = 6.4$ Hz, $J_3 = 2.6$ Hz), 5.17 (s, 2H), 4.76 (s, 2H), 3.87 (s, 3H) ppm; ^{13}C NMR (101 MHz, DMSO-d_6) δ 166.1, 145.1, 138.4, 138.0, 132.2, 129.8, 128.9, 128.4, 127.9, 121.4, 116.2, 114.2, 112.4, 68.8, 52.2 ppm; MS (ESI+) m/z = 258.1 $[M+H]^+$.

4.1.11. Methyl 3-((2-(3,4-dichloro-5-methyl-1H-pyrrole-2-carboxamido) phenoxy)methyl)benzoate (9) [26]

The synthesis was performed in accordance with general procedure C using compound **8** (1.70 g, 6.60 mmol) as starting material. The residue was co-evaporated with toluene and then washed with a mixture of methanol and ethyl acetate to give clean product. Yield: 86 % (2.45 g); grey amorphous solid; ^{1}H NMR (400 MHz, DMSO-d_6) δ 12.35 (s, 1H), 9.04 (s, 1H), 8.39 (dd, $J_1 = 8.0$ Hz, $J_2 = 1.7$ Hz, 1H), 8.14 (t, $J = 1.8$ Hz, 1H), 7.99 (dt, $J_1 = 7.8$ Hz, $J_2 = 1.5$ Hz, 1H), 7.82 (dt, $J_1 = 7.7$ Hz, $J_2 = 1.6$ Hz, 1H), 7.60 (t, $J = 7.7$ Hz, 1H), 7.25 (dd, $J_1 = 8.2$ Hz, $J_2 = 1.5$ Hz, 1H), 7.11 (td, $J_1 = 7.8$ Hz, $J_2 = 1.7$ Hz, 1H), 7.01 (td, $J_1 = 7.8$ Hz, $J_2 = 1.5$ Hz, 1H), 5.29 (s, 2H), 3.86 (s, 3H), 2.19 (s, 3H); ^{13}C NMR (101 MHz, DMSO-d_6) δ 166.0, 156.2, 146.9, 137.1, 133.5, 129.9, 129.3, 129.1, 129.1, 127.6, 126.3, 123.8, 121.1, 119.2, 118.8, 112.1, 109.5, 108.4, 69.8, 52.2, 10.7 ppm; MS (ESI+) m/z = 455.2 $[M+Na]^+$.

4.1.12. 3-((2-(3,4-Dichloro-5-methyl-1H-pyrrole-2-carboxamido) phenoxy)methyl)benzoic acid (10) [26]

The synthesis was performed in accordance with general procedure D using compound **9** (2.40 g, 5.54 mmol) as starting material. Yield: 95 % (2.45 g); grey amorphous solid; ^{1}H NMR (400 MHz, DMSO-d_6) δ 13.15 (s, 1H), 12.35 (s, 1H), 9.05 (s, 1H), 8.40 (dd, $J_1 = 8.1$ Hz, $J_2 = 1.7$ Hz, 1H), 8.11 (t, $J = 1.8$ Hz, 1H), 7.97 (dt, $J_1 = 7.8$ Hz, $J_2 = 1.4$ Hz, 1H), 7.77 (dt, $J_1 = 7.7$ Hz, $J_2 = 1.5$ Hz, 1H), 7.55 (t, $J = 7.7$ Hz, 1H), 7.25 (dd, $J_1 = 8.3$ Hz, $J_2 = 1.5$ Hz, 1H), 7.11 (td, $J_1 = 7.8$ Hz, $J_2 = 1.7$ Hz, 1H), 7.01 (td, $J_1 = 7.7$ Hz, $J_2 = 1.3$ Hz, 1H), 5.27 (s, 2H), 2.19 (s, 3H); ^{13}C NMR (101 MHz, DMSO-d_6) δ 167.7, 156.3, 147.0, 136.2, 133.8, 131.9, 129.5, 129.3, 129.2, 128.4, 127.6, 123.8, 121.0, 119.2, 118.8, 112.0, 109.6, 108.4, 70.2, 10.7 ppm; MS (ESI+) m/z = 441.2 $[M+Na]^+$.

4.1.13. tert-Butyl 4-(3-((2-(3,4-dichloro-5-methyl-1H-pyrrole-2-carboxamido)phenoxy)methyl)benzoyl)piperazine-1-carboxylate (11)

The synthesis was performed in accordance with general procedure E using compound **10** (0.200 g, 0.477 mmol) as starting material. Yield: 71 % (0.198 g); brown amorphous solid; ^{1}H NMR (400 MHz, DMSO-d_6) δ 12.36 (s, 1H), 9.05 (s, 1H), 8.38 (dd, 1H, $J_1 = 8.0$ Hz, $J_2 = 1.6$ Hz), 7.63 (dt, 1H, $J_1 = 7.7$ Hz, $J_2 = 1.5$ Hz), 7.58 (t, 1H, $J = 1.8$ Hz), 7.52 (t, 1H, $J = 7.6$ Hz), 7.44 (dt, 1H, $J_1 = 7.6$ HZ, $J_2 = 1.5$ Hz), 7.25 (dd, 1H, $J_1 = 8.2$ Hz, $J_2 = 1.4$ Hz), 7.11 (td, 1H, $J_1 = 7.8$ Hz, $J_2 = 1.7$ Hz), 7.01 (td, 1H, $J_1 = 7.7$ Hz, $J_2 = 1.3$ Hz), 5.24 (s, 2H), 3.59 (br s, 2H), 3.34 (br s, 6H), 2.19 (s, 3H), 1.40 (s, 9H); MS (ESI-) m/z = 586.4 $[M-H]^-$.

4.1.14. tert-Butyl 4-(3-((2-(3,4-dichloro-5-methyl-1H-pyrrole-2-carboxamido)phenoxy)methyl)benzamido)piperidine-1-carboxylate (12)

The synthesis was performed in accordance with general procedure E using compound **10** (0.152 g, 0.363 mmol) as starting material. Yield: 81 % (0.176 g); light grey amorphous solid; ^{1}H NMR (400 MHz, DMSO-d_6) δ 12.34 (s, 1H), 9.05 (s, 1H), 8.41 (dd, 1H, $J_1 = 8.0$ Hz, $J_2 = 1.6$ Hz), 8.33 (d, 1H, $J = 7.9$ Hz), 8.05 (t, 1H, $J = 1.9$ Hz), 7.87 (dt, 1H, $J_1 = 7.8$ Hz, $J_2 = 1.4$ Hz), 7.68 (dt, 1H, $J_1 = 7.8$ Hz, $J_2 = 1.3$ Hz), 7.52 (t, 1H, $J = 7.7$ Hz), 7.27 (dd, 1H, $J_1 = 8.3$ Hz, $J_2 = 1.4$ Hz), 7.11 (td, 1H, $J_1 = 7.8$ Hz, $J_2 = 1.7$ Hz), 7.01 (td, 1H, $J_1 = 7.7$ Hz, $J_2 = 1.3$ Hz), 5.24 (s, 2H), 4.05–3.85 (m, 3H), 2.84 (br s, 2H), 2.19 (s, 3H), 1.79 (d, 2H, J = 12.6 Hz), 1.40 (br s, 11*H*) ppm; MS (ESI+) m/z = 623.5 $[M+Na]^+$.

4.1.15. tert-Butyl (1-(3-((2-(3,4-dichloro-5-methyl-1H-pyrrole-2-carboxamido)phenoxy)methyl)benzoyl)piperidin-4-yl)carbamate (13)

The synthesis was performed in accordance with general procedure E using compound **10** (0.200 g, 0.477 mmol) as starting material. Yield: 55 % (0.158 g); grey amorphous solid; ^{1}H NMR (400 MHz, DMSO-d_6) δ 12.35 (s, 1H), 9.05 (s, 1H), 8.38 (dd, 1H, $J_1 = 8.0$ Hz, $J_2 = 1.5$ Hz), 7.61 (d, 1H, $J = 7.7$ Hz), 7.55–7.47 (m, 2H), 7.38 (d, 1H, $J = 7.7$ Hz), 7.29–7.22 (m, 1H), 7.11 (td, 1H, $J = 7.8$, 1.6 Hz), 7.05–6.97 (m, 1H), 6.86 (d, 1H, $J = 7.6$ Hz), 5.23 (s, 2H), 4.30 (s, 1H), 3.51 (s, 2H), 3.09 (br s, 1H), 2.93 (br s, 1H), 2.19 (s, 3H), 1.78 (br s, 1H), 1.66 (br s, 1H), 1.37 (s, 9H), 1.23 (br s, 2H) ppm; MS (ESI+) m/z = 623.5 $[M+Na]^+$.

4.1.16. tert-Butyl (1-(3-((2-(3,4-dichloro-5-methyl-1H-pyrrole-2-carboxamido)phenoxy)methyl)benzoyl)piperidin-4-yl)(methyl)carbamate (14)

The synthesis was performed in accordance with general procedure F using compound **10** (0.190 g, 0.453 mmol) as starting material. The product was further purified by column chromatography employing DCM/MeOH = 20/1 as the mobile phase. Yield: 83 % (0.230 g); off-white amorphous solid; ^{1}H NMR (400 MHz, DMSO-d_6) δ 12.36 (s, 1H), 9.06 (s, 1H), 8.38 (dd, $J_1 = 8.0$ Hz, $J_2 = 1.7$ Hz, 1H), 7.62 (dt, $J_1 = 7.6$ Hz, $J_2 = 1.6$ Hz, 1H), 7.57–7.48 (m, 2H), 7.44 (dt, $J_1 = 7.6$ Hz, $J_2 = 1.5$ Hz, 1H), 7.25 (dd, $J_1 = 8.3$ Hz, $J_2 = 1.4$ Hz, 1H), 7.10 (td, $J_1 = 7.8$ Hz, $J_2 = 1.6$ Hz, 1H), 7.00 (td, $J_1 = 7.8$ Hz, $J_2 = 1.5$ Hz, 1H), 5.24 (s, 2H), 4.57 (br s, 1H), 4.12–3.82 (m, 1H), 3.63 (br s, 1H), 3.07 (br s, 1H), 2.81–2.70 (m, 1H), 2.64 (s, 3H), 2.19 (s, 3H), 1.60 (br s, 3H), 1.39 (br s, 10*H*) ppm; MS (ESI+) m/z = 614.8 $[M+H]^+$.

4.1.17. tert-Butyl 3-((3-((2-(3,4-dichloro-5-methyl-1H-pyrrole-2-carboxamido)phenoxy)methyl)benzamido)methyl)piperidine-1-carboxylate (15)

The synthesis was performed in accordance with general procedure E using compound **10** (0.250 g, 0.596 mmol) as starting material. Yield: 49 % (0.223 g); brown amorphous solid; ^{1}H NMR (400 MHz, DMSO-d_6) δ 12.34 (s, 1H), 9.06 (s, 1H), 8.57 (t, 1H, $J = 5.8$ Hz), 8.41 (dd, 1H, $J_1 = 8.0$ Hz, $J_2 = 1.6$ Hz), 8.03 (s, 1H), 7.88 (dt, 1H, $J_1 = 7.8$ Hz, $J_2 = 1.5$ Hz), 7.69 (dt, 1H, $J_1 = 7.8$ Hz, $J_2 = 1.4$ Hz), 7.53 (t, 1H, $J = 7.7$ Hz), 7.26 (dd, 1H, $J_1 = 8.2$ Hz, $J_2 = 1.4$ Hz), 7.11 (td, 1H, $J_1 = 7.8$ Hz, $J_2 = 1.7$ Hz), 7.01 (td, 1H, $J_1 = 7.7$ Hz, $J_2 = 1.3$ Hz), 5.24 (s, 2H), 3.83 (br s, 1H), 3.74 (d, 1H, $J = 13.0$ Hz), 3.16 (t, 2H, $J = 6.4$ Hz), 2.83–2.72 (m, 1H), 1.80–1.65 (m, 2H), 1.65–1.64 (m, 1H), 1.32 (br s, 11*H*), 1.16 (br s, 1H) ppm; MS (ESI+) m/z = 637.5 $[M+Na]^+$.

4.1.18. tert-Butyl (3-(3-((2-(3,4-dichloro-5-methyl-1H-pyrrole-2-carboxamido)phenoxy)methyl)benzamido)propyl)carbamate (16)

The synthesis was performed in accordance with general procedure E using compound **10** (0.151 g, 0.360 mmol) as starting material. Yield: 73 % (0.152 g); light grey amorphous solid; ^{1}H NMR (400 MHz,

DMSO-d_6) δ 12.33 (s, 1H), 9.06 (s, 1H), 8.50 (t, 1H, J = 5.7 Hz), 8.41 (dd, 1H, J_1 = 8.0 Hz, J_2 = 1.6 Hz), 8.02 (d, 1H, J = 1.8 Hz), 7.87 (dt, 1H, J_1 = 7.9 Hz, J_2 = 1.4 Hz), 7.69 (dt, 1H, J_1 = 7.7 Hz, J_2 = 1.4 Hz), 7.53 (t, 1H, J = 7.7 Hz), 7.26 (dd, 1H, J_1 = 8.3 Hz, J_2 = 1.4 Hz), 7.11 (td, 1H, J_1 = 7.8 Hz, J_2 = 1.7 Hz), 7.01 (td, 1H, J_1 = 7.7 Hz, J_2 = 1.3 Hz), 6.81 (t, 1H, J = 5.8 Hz), 5.24 (s, 2H), 3.26 (q, 2H, J = 6.6 Hz), 2.97 (q, 2H, J = 6.6 Hz), 2.19 (s, 3H), 1.63 (p, 2H, J = 7.0 Hz), 1.36 (s, 9H) ppm; MS (ESI-) m/z = 573.4 $[M-H]^-$.

4.1.19. tert-Butyl 7-(3-((2-(3,4-dichloro-5-methyl-1H-pyrrole-2-carboxamido)phenoxy)methyl)benzoyl)-2,7-diazaspiro[4.4]nonane-2-carboxylate (17)

The synthesis was performed in accordance with general procedure F using compound **10** (0.190 g, 0.453 mmol) as starting material. The product was further purified by column chromatography employing DCM/MeOH = 20/1 as the mobile phase. Yield: 54 % (0.152 g); off-white amorphous solid; ^{1}H NMR (400 MHz, DMSO-d_6) δ 12.35 (s, 1H), 9.05 (d, J = 3.3 Hz, 1H), 8.38 (dd, J_1 = 7.9 Hz, J_2 = 1.7 Hz, 1H), 7.73–7.47 (m, 4H), 7.25 (dd, J_1 = 8.1 Hz, J_2 = 3.9 Hz, 1H), 7.14–7.05 (m, 1H), 7.00 (t, J = 7.8 Hz, 1H), 5.25 (s, 2H), 3.61–3.37 (m, 4H), 3.29–3.10 (m, 4H), 2.22–2.16 (m, 3H), 1.93–1.59 (m, 4H), 1.43–1.31 (m, 9H); MS (ESI+) m/z = 626.6 $[M+H]^+$.

4.1.20. tert-Butyl 3-(3-((2-(3,4-dichloro-5-methyl-1H-pyrrole-2-carboxamido)phenoxy)methyl)-N-methylbenzamido)piperidine-1-carboxylate (18)

The synthesis was performed in accordance with general procedure F using compound **10** (0.241 g, 0.574 mmol) as starting material. Yield: 90 % (0.317 g); brown amorphous solid; ^{1}H NMR (400 MHz, DMSO-d_6) δ 12.34 (s, 1H), 9.06 (s, 1H), 8.38 (dd, J_1 = 7.9 Hz, J_2 = 1.7 Hz, 1H), 7.66–7.36 (m, 4H), 7.23 (s, 1H), 7.14–7.06 (m, 1H), 7.00 (td, J_1 = 7.7 Hz, J_2 = 1.3 Hz, 1H), 5.24 (s, 2H), 4.34–3.66 (m, 4H), 2.98–2.75 (m, 4H), 2.20 (s, 3H), 1.75 (s, 3H), 1.49–1.19 (m, 11*H*) ppm; MS (ESI+) m/z = 615.4 $[M+H]^+$.

4.1.21. tert-Butyl (S)-3-(3-((2-(3,4-dichloro-5-methyl-1H-pyrrole-2-carboxamido)phenoxy)methyl)benzamido)piperidine-1-carboxylate (19)

The synthesis was performed in accordance with general procedure F using compound **10** (0.224 g, 0.534 mmol) as starting material. Yield: 84 % (0.271 g); grey amorphous solid; ^{1}H NMR (400 MHz, DMSO-d_6) δ 12.34 (s, 1H), 9.05 (s, 1H), 8.41 (dd, J_1 = 8.0 Hz, J_2 = 1.7 Hz, 1H), 8.31 (d, J = 6.8 Hz, 1H), 8.04 (s, 1H), 7.88 (d, J = 7.9 Hz, 1H), 7.69 (dt, J_1 = 7.6 Hz, J_2 = 1.4 Hz, 1H), 7.53 (t, J = 7.6 Hz, 1H), 7.26 (dd, J_1 = 8.3 Hz, J_2 = 1.3 Hz, 1H), 7.11 (td, J_1 = 7.8 Hz, J_2 = 1.7 Hz, 1H), 7.01 (td, J_1 = 7.7 Hz, J_2 = 1.3 Hz, 1H), 5.24 (s, 2H), 3.96–3.70 (m, 3H), 2.83–2.71 (m, 1H), 2.19 (s, 3H), 1.92–1.86 (m, 1H), 1.78–1.62 (m, 1H), 1.59–1.29 (m, 12H) ppm; MS (ESI-) m/z = 599.4 $[M-H]^-$.

4.1.22. tert-Butyl (R)-3-(3-((2-(3,4-dichloro-5-methyl-1H-pyrrole-2-carboxamido)phenoxy)methyl)benzamido)piperidine-1-carboxylate (20)

The synthesis was performed in accordance with general procedure F using compound **10** (0.209 g, 0.499 mmol) as starting material. Yield: 83 % (0.248 g); brown amorphous solid; ^{1}H NMR (400 MHz, DMSO-d_6) δ 12.34 (s, 1H), 9.05 (s, 1H), 8.41 (dd, J_1 = 8.1 Hz, J_2 = 1.7 Hz, 1H), 8.31 (d, J = 7.2 Hz, 1H), 8.04 (s, 1H), 7.88 (d, J = 7.8 Hz, 1H), 7.69 (dt, J_1 = 7.6 Hz, J_2 = 1.4 Hz, 1H), 7.53 (t, J = 7.6 Hz, 1H), 7.27 (dd, J_1 = 8.3 Hz, J_2 = 1.5 Hz, 1H), 7.11 (td, J_1 = 7.8 Hz, J_2 = 1.7 Hz, 1H), 7.01 (td, J_1 = 7.8 Hz, J_2 = 1.4 Hz, 1H), 5.24 (s, 2H), 3.95–3.66 (m, 3H), 2.82–2.74 (m, 1H), 2.19 (s, 3H), 1.92–1.86 (m, 1H), 1.75–1.68 (m, 1H), 1.37 (br s, 12H) ppm; ^{13}C NMR (101 MHz, DMSO-d_6) δ 165.5, 156.2, 153.9, 146.9, 136.3, 134.6, 131.5, 129.3, 128.4, 127.8, 127.6, 127.4, 123.8, 121.0, 119.1, 118.8, 111.9, 109.6, 108.4, 78.7, 70.2, 46.0, 29.7, 28.0, 10.7 ppm; MS (ESI+) m/z = 601.4 $[M+Na]^+$.

4.1.23. Ethyl 1-(3-((2-(3,4-dichloro-5-methyl-1H-pyrrole-2-carboxamido)phenoxy)methyl)benzoyl)piperidine-4-carboxylate (21)

The synthesis was performed in accordance with general procedure F using compound **10** (0.200 g, 0.477 mmol) as starting material. The product was further purified by column chromatography employing DCM/MeOH = 20/1 as the mobile phase. Yield: 82 % (0.217 g); off-white amorphous solid; ^{1}H NMR (400 MHz, DMSO-d_6) δ 12.35 (s, 1H), 9.05 (s, 1H), 8.38 (dd, J_1 = 8.0 Hz, J_2 = 1.7 Hz, 1H), 7.64–7.57 (m, 1H), 7.57–7.46 (m, 2H), 7.41 (dt, J_1 = 7.6 Hz, J_2 = 1.5 Hz, 1H), 7.25 (dd, J_1 = 8.3 Hz, J_2 = 1.4 Hz, 1H), 7.11 (td, J_1 = 7.8 Hz, J_2 = 1.7 Hz, 1H), 7.00 (td, J_1 = 7.7 Hz, J_2 = 1.4 Hz, 1H), 5.24 (s, 2H), 4.32 (s, 1H), 4.06 (q, J = 7.2 Hz, 2H), 3.55 (br s, 1H), 3.20–2.88 (m, 2H), 2.65–2.57 (m, 1H), 2.19 (s, 3H), 1.95–1.68 (m, 2H), 1.51 (br s, 2H), 1.17 (t, J = 7.1 Hz, 3H) ppm; ^{13}C NMR (101 MHz, DMSO-d_6) δ 173.7, 168.7, 156.2, 146.9, 136.6, 136.4, 129.8, 129.3, 128.6, 127.6, 127.1, 126.7, 123.7, 121.0, 119.1, 118.8, 112.0, 109.4, 108.4, 70.0, 60.0, 46.3, 40.7, 28.3, 27.5, 14.1, 10.7 ppm; HRMS calcd. for $C_{28}H_{30}O_5N_3Cl_2$ ($[M+H]^+$): 558.15570, found 558.15581; UHPLC: t_r = 5.903 min (99.4 % at 254 nm).

4.1.24. 4-(3-((2-(3,4-Dichloro-5-methyl-1H-pyrrole-2-carboxamido)phenoxy)methyl)benzoyl)piperazin-1-ium chloride (22)

The synthesis was performed in accordance with general procedure G using compound **11** (0.167 g, 0.284 mmol) as starting material. Yield: 87 % (0.129 g); grey amorphous solid; ^{1}H NMR (400 MHz, DMSO-d_6) δ 12.37 (s, 1H), 9.06 (s, 1H), 9.20 (s, 2H), 8.39 (dd, 1H, J_1 = 8.0 Hz, J_2 = 1.6 Hz), 7.72–7.61 (m, 2H), 7.53 (q, 2H, J = 7.4 Hz), 7.25 (dd, 1H, J_1 = 8.2 Hz, J_2 = 1.1 Hz), 7.11 (td, 1H, J_1 = 7.9 Hz, J_2 = 1.6 Hz), 7.06–6.96 (m, 1H), 5.24 (s, 2H), 3.94–3.49 (m, 4H), 3.15 (br s, 4H), 2.20 (s, 3H); ^{13}C NMR (101 MHz, DMSO-d_6) δ 168.9, 156.2, 147.0, 136.7, 135.0, 130.3, 129.3, 128.7, 127.63, 127.60, 127.1, 123.8, 121.1, 119.2, 118.8, 112.0, 109.5, 108.4, 70.0, 42.4, 10.7 ppm; HRMS calcd. for $C_{24}H_{25}O_3N_4Cl_2$ ($[M+H]^+$): 487.12982, found 487.12816; UHPLC: t_r = 3.957 min (96.7 % at 254 nm).

4.1.25. 4-(3-((2-(3,4-Dichloro-5-methyl-1H-pyrrole-2-carboxamido)phenoxy)methyl)benzamido)piperidin-1-ium chloride (23)

The synthesis was performed in accordance with general procedure G using compound **12** (0.135 g, 0.224 mmol) as starting material. Yield: 98 % (0.119 g); light grey amorphous solid; ^{1}H NMR (400 MHz, DMSO-d_6) δ 12.36 (s, 1H), 9.06 (s, 1H), 8.93–8.74 (m, 2H), 8.58 (d, 1H, J = 7.5 Hz), 8.41 (dd, 1H, J_1 = 8.0 Hz, J_2 = 1.6 Hz), 8.08 (s, 1H), 7.92 (d, 1H, J = 7.9 Hz), 7.70 (d, 1H, J = 7.7 Hz), 7.53 (t, 1H, J = 7.7 Hz), 7.27 (dd, 1H, J_1 = 8.2 Hz, J_2 = 1.1 Hz), 7.12 (td, 1H, J_1 = 7.9 Hz, J_2 = 1.6 Hz), 7.06–6.97 (m, 1H), 5.25 (s, 2H), 4.18–4.01 (m, 1H), 3.30 (d, 2H, J = 12.8 Hz), 3.00 (q, 2H, J = 11.9 Hz), 2.20 (s, 3H), 1.97 (d, 2H, J = 11.0 Hz), 1.86–1.71 (m, 2H) ppm; ^{13}C NMR (101 MHz, DMSO-d_6) δ 165.5, 156.2, 146.9, 136.3, 134.5, 131.5, 129.3, 128.4, 127.9, 127.6, 127.5, 123.8, 121.0, 119.2, 118.8, 111.9, 109.6, 108.4, 70.1, 44.5, 42.2, 28.2, 10.7 ppm; HRMS calcd. for $C_{25}H_{27}O_3N_4Cl_2$ ($[M+H]^+$): 501.14547, found 501.14358; UHPLC: t_r = 4.070 min (98.6 % at 254 nm).

4.1.26. 1-(3-((2-(3,4-Dichloro-5-methyl-1H-pyrrole-2-carboxamido)phenoxy)methyl)benzoyl)piperidin-4-aminium chloride (24)

The synthesis was performed in accordance with general procedure G using compound **13** (0.118 g, 0.196 mmol) as starting material. Yield: 85 % (90 mg); light grey amorphous solid; ^{1}H NMR (400 MHz, DMSO-d_6) δ 12.37 (s, 1H), 9.06 (s, 1H), 8.38 (dd, 1H, J_1 = 8.0 Hz, J_2 = 1.6 Hz), 8.23 (s, 3H), 7.64 (dt, 1H, J_1 = 7.7 Hz, J_2 = 1.3 Hz), 7.57–7.50 (m, 2H), 7.40 (dt, 1H, J_1 = 7.6 Hz, J_2 = 1.4 Hz), 7.25 (dd, 1H, J_1 = 8.3 Hz, J_2 = 1.4 Hz), 7.11 (td, 1H, J_1 = 7.8 Hz, J_2 = 1.7 Hz), 7.01 (td, 1H, J_1 = 7.7 Hz, J_2 = 1.3 Hz), 5.24 (s, 2H), 4.47 (br s, 1H), 3.65 (br s, 1H), 3.34–3.24 (m, 1H), 3.21–2.81 (m, 2H), 2.20 (s, 3H), 2.09–1.73 (m, 2H) 1.50 (br s, 2H) ppm; ^{13}C NMR (101 MHz, DMSO-d_6) δ 168.8, 162.3, 156.2, 147.0, 136.7, 136.1, 130.1, 129.3, 128.7, 127.6, 127.2, 126.6, 123.8, 121.1, 119.1, 118.8, 112.0, 109.5, 108.4, 70.0, 47.3, 34.1, 30.0, 10.7 ppm; HRMS calcd. for $C_{25}H_{27}O_3N_4Cl_2$ ($[M+H]^+$): 501.14547,

found 501.14381; UHPLC: t_r = 3.960 min (98.2 % at 254 nm).

4.1.27. 3,4-Dichloro-5-methyl-N-(2-((3-(4-(methylamino)piperidine-1-carbonyl)benzyl)oxy)phenyl)-1H-pyrrole-2-carboxamide (25)

The synthesis was performed in accordance with general procedure H using compound **14** (0.100 g, 0.162 mmol) as starting material. Upon completion the product was purified by column chromatography employing DCM/MeOH/NH_4OH = 12/1/0.1 as the mobile phase. Yield: 80 % (0.067 g); white amorphous solid; ^{1}H NMR (400 MHz, DMSO-d_6) δ 9.07 (s, 1H), 8.38 (dd, J_1 = 8.1 Hz, J_2 = 1.7 Hz, 1H), 7.64–7.56 (m, 1H), 7.55–7.46 (m, 2H), 7.39 (dt, J_1 = 7.6 Hz, J_2 = 1.4 Hz, 1H), 7.25 (dd, J_1 = 8.2 Hz, J_2 = 1.5 Hz, 1H), 7.10 (td, J_1 = 7.7 Hz, J_2 = 1.7 Hz, 1H), 7.00 (td, J_1 = 7.7 Hz, J_2 = 1.3 Hz, 1H), 5.23 (s, 2H), 4.32–4.14 (m, 1H), 3.53 (br s, 1H), 3.11–2.90 (m, 2H), 2.25 (s, 3H), 2.19 (s, 3H), 2.00–1.63 (m, 2H), 1.36–0.81 (m, 2H) ppm, signal for the remaining aliphatic proton is overlapped with water in DMSO signal; ^{13}C NMR (101 MHz, DMSO-d_6) δ 168.5, 156.2, 146.9, 136.6, 136.6, 129.7, 129.3, 128.6, 127.7, 127.0, 126.6, 123.7, 121.0, 119.1, 118.8, 112.0, 109.4, 108.3, 70.0, 55.6, 45.6, 33.0, 31.7, 31.1, 10.7 ppm; HRMS calcd. for $C_{26}H_{29}O_3N_4Cl_2$ ([M+H]$^+$): 515.16112, found 515.16117; UHPLC: t_r = 4.327 min (99.4 % at 254 nm).

4.1.28. 3-((3-((2-(3,4-Dichloro-5-methyl-1H-pyrrole-2-carboxamido)phenoxy)methyl)benzamido)methyl)piperidin-1-ium chloride (26)

The synthesis was performed in accordance with general procedure G using compound **15** (0.152 g, 0.363 mmol) as starting material. The residue was washed with methanol instead of acetonitrile. Yield: 31 % (0.039 g); light brown amorphous solid; ^{1}H NMR (400 MHz, DMSO-d_6) δ 12.36 (s, 1H), 9.06 (s, 1H), 8.81 (d, 1H, J = 11.3 Hz), 8.71 (t, 1H, J = 5.9 Hz), 8.58–8.47 (m, 1H), 8.40 (dd, 1H, J_1 = 8.0 Hz, J_2 = 1.7 Hz), 8.04 (t, 1H, J = 1.8 Hz), 7.91 (dt, 1H, J_1 = 7.8 Hz, J_2 = 1.5 Hz), 7.71 (dt, 1H, J_1 = 7.7 Hz, J_2 = 1.4 Hz), 7.55 (t, 1H, J = 7.7 Hz), 7.26 (dd, 1H, J_1 = 8.3 Hz, J_2 = 1.3 Hz), 7.11 (td, 1H, J_1 = 7.8 Hz, J_2 = 1.7 Hz), 7.01 (td, 1H, J_1 = 7.8 Hz, J_2 = 1.3 Hz), 5.25 (s, 2H), 3.25–3.15 (m, 4H), 2.75 (q, 1H, J = 11.6 Hz), 2.67–2.56 (m, 1H), 2.19 (s, 3H), 2.01 (br s, 1H), 1.77 (d, 2H, J = 12.5 Hz), 1.67–1.52 (m, 1H), 1.22 (q, 1H, J = 11.5 Hz) ppm; ^{13}C NMR (101 MHz, DMSO-d_6) δ 166.1, 156.2, 147.0, 136.4, 134.4, 131.6, 129.3, 128.5, 127.8, 127.6, 127.2, 123.8, 121.0, 119.2, 118.8, 111.9, 109.6, 108.4, 70.2, 46.4, 43.3, 42.0, 33.8, 26.1, 21.4, 10.7 ppm; HRMS calcd. for $C_{26}H_{29}O_3N_4Cl_2$ ([M+H]$^+$): 515.16112, found 515.15951; UHPLC: t_r = 4.137 min (97.0 % at 254 nm).

4.1.29. 3-(3-((2-(3,4-Dichloro-5-methyl-1H-pyrrole-2-carboxamido)phenoxy)methyl)benzamido)propan-1-aminium chloride (27)

The synthesis was performed in accordance with general procedure G using compound **16** (0.123 g, 0.214 mmol) as starting material. Yield: 90 % (0.099 g); light grey amorphous solid; ^{1}H NMR (400 MHz, DMSO-d_6) δ 12.36 (s, 1H), 9.06 (s, 1H), 8.78 (t, 1H, J = 5.8 Hz), 8.40 (dd, 1H, J_1 = 8.0 Hz, J_2 = 1.6 Hz), 8.05 (d, 1H, J = 1.8 Hz), 7.98–7.82 (m, 4H), 7.71 (dt, 1H, J_1 = 7.7 Hz, J_2 = 1.4 Hz), 7.54 (t, 1H, J = 7.7 Hz), 7.26 (dd, 1H, J_1 = 8.3 Hz, J_2 = 1.4 Hz), 7.11 (td, 1H, J_1 = 7.8 Hz, J_2 = 1.7 Hz), 7.01 (td, 1H, J_1 = 7.7 Hz, J_2 = 1.3 Hz), 5.25 (s, 2H), 3.35 (q, 2H, J = 6.4 Hz), 2.84 (dd, 2H, J = 7.7, 7.1 Hz), 2.19 (s, 3H), 1.82 (p, 2H, J = 6.9 Hz) ppm; ^{13}C NMR (101 MHz, DMSO-d_6) δ 166.1, 156.2, 147.0, 136.4, 134.4, 131.6, 129.3, 128.5, 127.7, 127.6, 127.2, 123.8, 121.0, 119.2, 118.8, 111.9, 109.6, 108.4, 70.2, 36.7, 36.2, 27.3, 10.7 ppm; HRMS calcd for $C_{23}H_{25}O_3N_4Cl_2$ ([M+H]$^+$): 475.12982, found 475.12835; HPLC: t_r = 4.013 min (97.9 % at 254 nm).

4.1.30. N-(2-((3-(2,7-Diazaspiro[4.4]nonane-2-carbonyl)benzyl)oxy)phenyl)-3,4-dichloro-5-methyl-1H-pyrrole-2-carboxamide (28)

The synthesis was performed in accordance with general procedure H using compound **17** (0.083 g, 0.132 mmol) as starting material. Upon completion product was purified by column chromatography employing DCM/MeOH/NH_4OH = 15/1/0.1 as the mobile phase. Yield: 43 % (0.032 g); white amorphous solid; ^{1}H NMR (400 MHz, DMSO-d_6) δ 9.07 (d, J = 2.7 Hz, 1H), 8.38 (d, J = 7.9 Hz, 1H), 7.70–7.59 (m, 2H), 7.52 (dq, J_1 = 15.0 Hz, J_2 = 7.6 Hz, 2H), 7.29–7.22 (m, 1H), 7.15–7.06 (m, 1H), 7.00 (t, J = 7.5 Hz, 1H), 5.25 (s, 2H), 3.00–2.57 (m, 4H), 2.19 (s, 3H), 1.91–1.43 (m, 4H) ppm, the remaining four aliphatic protons are overlapped with water in DMSO signals; ^{13}C NMR (101 MHz, DMSO-d_6) δ 168.2, 167.9, 156.2, 146.9, 137.0, 136.8, 136.5, 130.3, 130.0, 129.3, 128.5, 128.5, 127.3, 127.1, 123.7, 121.0, 119.3, 119.1, 118.8, 112.1, 109.5, 108.4, 70.0, 57.8, 55.0, 53.8, 53.7, 49.3, 48.1, 47.4, 45.3, 44.9, 44.7, 35.3, 34.7, 34.4, 33.8, 10.7 ppm, rotamers are present in the spectra; HRMS calcd. for $C_{27}H_{29}O_3N_4Cl_2$ ([M+H]$^+$): 527.16112, found 527.16110; UHPLC: t_r = 4.353 min (96.7 % at 254 nm).

4.1.31. 3,4-Dichloro-5-methyl-N-(2-((3-(methyl(piperidin-3-yl)carbamoyl)benzyl)oxy)phenyl)-1H-pyrrole-2-carboxamide (29)

The synthesis was performed in accordance with general procedure H using compound **18** (0.100 g, 0.162 mmol) as starting material. Upon completion product was purified by column chromatography employing DCM/MeOH/NH_4OH = 15/1/0.1 as the mobile phase. Yield: 65 % (0.055 g); white amorphous solid; ^{1}H NMR (400 MHz, DMSO-d_6) δ 9.07 (s, 1H), 8.38 (dd, J_1 = 8.1 Hz, J_2 = 1.7 Hz, 1H), 7.67–7.45 (m, 3H), 7.44–7.35 (m, 1H), 7.25 (d, J = 7.0 Hz, 1H), 7.10 (td, J_1 = 7.8 Hz, J_2 = 1.7 Hz, 1H), 7.00 (td, J_1 = 7.7 Hz, J_2 = 1.3 Hz, 1H), 5.25 (s, 2H), 4.41–3.93 (m, 1H), 2.91–2.57 (m, 7H), 2.20 (s, 3H), 1.78–1.40 (m, 3.5H), 1.09 (br s, 0.5H) ppm; ^{13}C NMR (101 MHz, DMSO-d_6) δ 156.3, 146.9, 137.3, 136.6, 129.3, 128.8, 127.6, 125.8, 123.8, 121.0, 119.2, 118.8, 112.1, 109.5, 108.4, 69.6, 49.1, 48.2, 45.1, 32.3, 27.6, 26.1, 10.8 ppm, representative peaks are visible; HRMS calcd. for $C_{26}H_{29}O_3N_4Cl_2$ ([M+H]$^+$): 515.16112, found 515.16088; UHPLC: t_r = 4.497 min (100 % at 254 nm).

4.1.32. (S)-3,4-Dichloro-5-methyl-N-(2-((3-(piperidin-3-ylcarbamoyl)benzyl)oxy)phenyl)-1H-pyrrole-2-carboxamide (30)

The synthesis was performed in accordance with general procedure H using compound **19** (0.100 g, 0.166 mmol) as starting material. The product was purified by column chromatography employing DCM/MeOH/NH_4OH = 9/1/0.1 as the mobile phase. Yield: 76 % (0.063 g); white amorphous solid; ^{1}H NMR (400 MHz, DMSO-d_6) δ 9.07 (s, 1H), 8.41 (dd, J_1 = 8.1 Hz, J_2 = 1.7 Hz, 1H), 8.18 (d, J = 8.2 Hz, 1H), 8.04 (t, J = 1.8 Hz, 1H), 7.87 (dt, J_1 = 7.8 Hz, J_2 = 1.5 Hz, 1H), 7.68 (dt, J_1 = 7.6 Hz, J_2 = 1.5 Hz, 1H), 7.51 (t, J = 7.6 Hz, 1H), 7.26 (dd, J_1 = 8.3 Hz, J_2 = 1.4 Hz, 1H), 7.11 (td, J_1 = 7.8 Hz, J_2 = 1.7 Hz, 1H), 7.01 (td, J_1 = 7.8 Hz, J_2 = 1.4 Hz, 1H), 5.24 (s, 2H), 3.88–3.72 (m, 1H), 3.01–2.93 (m, 1H), 2.83–2.75 (m, 1H), 2.45–2.34 (m, 2H), 2.19 (s, 3H), 1.90–1.81 (m, 1H), 1.67–1.57 (m, 1H), 1.53–1.33 (m, 2H) ppm; ^{13}C NMR (101 MHz, DMSO-d_6) δ 165.3, 156.3, 146.9, 136.3, 134.9, 131.3, 129.3, 128.4, 127.7, 127.6, 127.3, 123.7, 121.0, 119.1, 118.8, 111.9, 109.6, 108.4, 70.2, 51.0, 46.9, 45.6, 30.6, 25.2, 10.8 ppm; HRMS calcd. for $C_{25}H_{27}O_3N_4Cl_2$ ([M+H]$^+$): 501.14547, found 501.14510; UHPLC: t_r = 4.440 min (99.2 % at 254 nm).

4.1.33. (R)-3,4-Dichloro-5-methyl-N-(2-((3-(piperidin-3-ylcarbamoyl)benzyl)oxy)phenyl)-1H-pyrrole-2-carboxamide (31)

The synthesis was performed in accordance with general procedure H using compound **20** (0.100 g, 0.166 mmol) as starting material. Upon completion the product was purified by column chromatography employing DCM/MeOH/NH_4OH = 9/1/0.1 as the mobile phase. Yield: 77 % (0.064 g); white amorphous solid; ^{1}H NMR (400 MHz, DMSO-d_6) δ 9.07 (s, 1H), 8.41 (dd, J_1 = 8.0 Hz, J_2 = 1.7 Hz, 1H), 8.18 (d, J = 8.1 Hz, 1H), 8.04 (t, J = 1.8 Hz, 1H), 7.87 (dt, J_1 = 7.8 Hz, J_2 = 1.5 Hz, 1H), 7.68 (dt, J_1 = 7.3 Hz, J_2 = 1.5 Hz, 1H), 7.51 (t, J = 7.7 Hz, 1H), 7.26 (dd, J_1 = 8.3 Hz, J_2 = 1.4 Hz, 1H), 7.11 (td, J_1 = 7.8 Hz, J_2 = 1.7 Hz, 1H), 7.01 (td, J_1 = 7.8 Hz, J_2 = 1.4 Hz, 1H), 5.24 (s, 2H), 3.87–3.72 (m, 1H), 2.97 (dd, J_1 = 12.0 Hz, J_2 = 3.2 Hz, 1H), 2.83–2.76 (m, 1H), 2.45–2.35 (m, 2H), 2.19 (s, 3H), 1.88–1.74 (m, 1H), 1.67–1.57 (m, 1H), 1.53–1.36 (m, 2H) ppm; ^{13}C NMR (101 MHz, DMSO-d_6) δ 165.3, 156.3, 146.9, 136.27, 134.8, 131.3, 129.3, 128.4, 127.7, 127.6, 127.3, 123.8, 121.0, 119.1,

118.8, 111.9, 109.6, 108.4, 70.2, 50.7, 46.7, 45.5, 30.4, 25.0, 10.7 ppm; HRMS calcd. for $C_{25}H_{27}O_3N_4Cl_2$ ([M+H]$^+$): 501.14547, found 501.14515; UHPLC: t_r = 4.437 min (99.2 % at 254 nm).

4.1.34. 1-(3-((2-(3,4-Dichloro-5-methyl-1H-pyrrole-2-carboxamido) phenoxy)methyl)benzoyl)piperidine-4-carboxylic acid (32)

The synthesis was performed in accordance with general procedure D using compound **21** (0.174 g, 0.312 mmol) as starting material. Yield: 93 % (0.153 g); white amorphous solid; ^{1}H NMR (400 MHz, DMSO-d_6) δ 12.40 (s, 1H), 9.08 (s, 1H), 8.36 (d, J = 7.7 Hz, 1H), 7.61 (d, J = 7.6 Hz, 1H), 7.56–7.45 (m, 2H), 7.40 (d, J = 8.2 Hz, 1H), 7.25 (d, J = 7.9 Hz, 1H), 7.14–7.06 (m, 1H), 7.04–6.95 (m, 1H), 5.24 (s, 2H), 4.39–4.19 (m, 1H), 3.53 (br s, 1H), 3.10–2.91 (m, 2H), 2.19 (s, 3H), 2.00–1.64 (m, 2H), 1.50 (br s, 2H) ppm, the remaining aliphatic proton is overlapped with water in DMSO signal; ^{13}C NMR (101 MHz, DMSO-d_6) δ 175.6, 168.6, 147.0, 136.6, 136.5, 129.7, 129.3, 128.6, 127.7, 127.1, 126.6, 123., 121.00, 119.2, 118.8, 112.1, 111.2, 109.5, 108.3, 70.0, 10.8 ppm, representative peaks are visible due to solubility limitations; HRMS calcd. for $C_{26}H_{26}O_5N_3Cl_2$ ([M+H]$^+$): 530.12440, found 530.12444; UHPLC: t_r = 5.027 min (98.2 % at 254 nm).

4.1.35. Methyl 3-((4-methoxy-2-nitrophenoxy)methyl)benzoate (33)

The synthesis was performed in accordance with general procedure A using 2-nitro-4-methoxyphenol (2.00 g, 11.8 mmol) as starting material. Yield: 62 % (2.13 g); yellow amorphous solid; ^{1}H NMR (400 MHz, $CDCl_3$) δ 8.09 (td, 1H, J_1 = 1.8 Hz, J_2 = 0.8 Hz), 8.04–7.98 (m, 1H), 7.75–7.69 (m, 1H), 7.49 (t, 1H, J = 7.7 Hz), 7.41 (dd, 1H, J_1 = 2.6 Hz, J_2 = 0.8 Hz), 7.10–7.03 (m, 2H), 5.21 (s, 2H), 3.93 (s, 3H), 3.82 (s, 3H) ppm; MS (ESI+) m/z = 340.2 ([M+Na]$^+$).

4.1.36. 3-((4-Methoxy-2-nitrophenoxy)methyl)benzoic acid (34)

The synthesis was performed in accordance with general procedure D using compound **33** (2.02 g, 6.36 mmol) as starting material. Yield: 96 % (1.86 g); yellow amorphous solid; ^{1}H NMR (400 MHz, DMSO-d_6) δ 13.05 (s, 1H), 8.04 (t, 1H, J = 1.8 Hz), 7.91 (dt, 1H, J_1 = 7.7 Hz, J_2 = 1.5 Hz), 7.68 (dt, 1H, J_1 = 7.8 Hz, J_2 = 1.4 Hz), 7.54 (t, 1H, J = 7.7 Hz), 7.48 (d, 1H, J = 3.1 Hz), 7.40 (d, 1H, J = 9.2 Hz), 7.26 (dd, 1H, J_1 = 9.2 Hz, J_2 = 3.1 Hz), 5.32 (s, 2H), 3.78 (s, 3H) ppm; MS (ESI+) m/z = 326.2 ([M+Na]$^+$).

4.1.37. tert-Butyl 3-(3-((4-methoxy-2-nitrophenoxy)methyl)benzamido) piperidine-1-carboxylate (35)

The synthesis was performed in accordance with general procedure E using compound **34** (1.00 g, 3.23 mmol) as starting material. Yield: 94 % (1.47 g); yellow amorphous solid; ^{1}H NMR (400 MHz, DMSO-d_6) δ 8.30 (d, 1H, J = 7.4 Hz), 7.90 (d, 1H, J = 2.1 Hz), 7.80 (d, 1H, J = 7.7 Hz), 7.59 (dt, 1H, J_1 = 7.8 Hz, J_2 = 1.4 Hz), 7.53–7.48 (m, 1H), 7.47 (d, 1H, J = 2.1 Hz), 7.39 (d, 1H, J = 9.2 Hz), 7.25 (dd, 1H, J_1 = 9.2 Hz, J_2 = 3.2 Hz), 5.29 (s, 2H), 3.86 (br s, 1H), 3.84–3.67 (m, 5H), 2.92 (br s, 1H), 2.79 (t, 1H, J = 12.0 Hz), 1.89 (d, 1H, J = 12.3 Hz), 1.73 (d, 1H, J = 12.9 Hz), 1.53 (q, 1H, J = 12.2 Hz), 1.33 (br s, 10*H*) ppm; MS (ESI+) m/z = 509.4 ([M+Na]$^+$).

4.1.38. tert-Butyl 3-(3-((2-amino-4-methoxyphenoxy)methyl)benzamido) piperidine-1-carboxylate (36)

The synthesis was performed in accordance with general procedure B using compound **35** (1.25 g, 2.58 mmol) as starting material. The product was further purified by flash column chromatography using EtOAc/Hexane = 1/1 as the mobile phase. Yield: 39 % (0.459 g); light brown amorphous solid; ^{1}H NMR (400 MHz, DMSO-d_6) δ 8.30 (d, 1H, J = 7.4 Hz), 7.92 (d, 1H, J = 1.8 Hz), 7.78 (d, 1H, J = 7.7 Hz), 7.62 (dt, 1H, J_1 = 7.9 Hz, J_2 = 1.3 Hz), 7.47 (t, 1H, J = 7.7 Hz), 6.75 (d, 1H, J = 8.8 Hz), 6.27 (d, 1H, J = 2.9 Hz), 6.04 (dd, 1H, J_1 = 8.7 Hz, J_2 = 3.0 Hz), 5.04 (s, 2H), 4.83 (s, 2H), 3.91 (br s, 1H), 3.83–3.69 (m, 2H), 3.61 (s, 3H), 2.92 (br s, 1H), 2.79 (t, 1H, J = 11.9 Hz), 1.94–1.83 (m, 1H), 1.73 (d, 1H, J = 12.9 Hz), 1.53 (q, 1H, J = 10.6 Hz), 1.38 (br s, 10*H*) ppm; MS (ESI+) m/z = 478.4 ([M+Na]$^+$).

4.1.39. tert-Butyl 3-(3-((2-(3,4-dichloro-5-methyl-1H-pyrrole-2-carboxamido)-4-methoxyphenoxy)methyl)benzamido)piperidine-1-carboxylate (37)

The synthesis was performed in accordance with general procedure C using compound **36** (0.371 g, 0.814 mmol) as starting material. The residue was taken up in EtOAc (50 mL) and water (25 mL) and the water phase was removed. The organic layer was additionally washed with 1 M $HCl_{(aq)}$ (3 × 20 mL) and saturated $NaHCO_{3(aq)}$ (3 × 20 mL). It was then washed with brine (3 × 20 mL), dried over Na_2SO_4, filtered, and the volatiles were evaporated under reduced pressure. The product was further purified by flash column chromatography using EtOAc/Hexane = 1/1 as the mobile phase. Yield: 42 % (0.216 g); light orange amorphous solid; ^{1}H NMR (400 MHz, DMSO-d_6) δ 12.36 (s, 1H), 9.05 (s, 1H), 8.31 (d, 1H, J = 7.5 Hz), 8.09 (d, 1H, J = 3.0 Hz), 8.02 (s, 1H), 7.87 (d, 1H, J = 7.8 Hz), 7.67 (dt, 1H, J_1 = 7.7 Hz, J_2 = 1.4 Hz), 7.52 (t, 1H, J = 7.7 Hz), 7.18 (d, 1H, J = 9.0 Hz), 6.67 (dd, 1H, J_1 = 8.9 Hz, J_2 = 3.1 Hz), 5.18 (s, 2H), 3.91 (br s, 1H), 3.83–3.73 (m, 2H), 3.73 (s, 3H), 2.88 (br s, 1H), 2.77 (t, 1H, J = 11.9 Hz), 2.19 (s, 3H), 1.94–1.83 (m, 1H), 1.72 (d, 1H, J = 9.3 Hz), 1.60–1.47 (m, 1H), 1.37 (br s, 10*H*) ppm; MS (ESI-) m/z = 631.5 ([M−H]$^-$).

4.1.40. 3-(3-((2-(3,4-Dichloro-5-methyl-1H-pyrrole-2-carboxamido)-4-methoxyphenoxy)methyl)benzamido)piperidin-1-ium chloride (38)

The synthesis was performed in accordance with general procedure G using compound **37** (0.170 g, 0.277 mmol) as starting material. Yield: 84 % (0.132 g); light grey amorphous solid; ^{1}H NMR (400 MHz, DMSO-d_6) δ 12.38 (s, 1H), 9.18 (d, 1H, J = 9.2 Hz), 9.05 (s, 1H), 8.92 (dd, 1H, J_1 = 19.0 Hz, J_2 = 9.9 Hz), 8.65 (d, 1H, J = 7.6 Hz), 8.12–8.04 (m, 2H), 7.94 (dt, 1H, J_1 = 7.8 Hz, J_2 = 1.5 Hz), 7.69 (dt, 1H, J_1 = 7.6 Hz, J_2 = 1.4 Hz), 7.53 (t, 1H, J = 7.7 Hz), 7.18 (d, 1H, J = 9.0 Hz), 6.68 (dd, 1H, J_1 = 9.0 Hz, J_2 = 3.1 Hz), 5.19 (s, 2H), 4.28–4.15 (m, 1H), 3.73 (s, 3H), 3.31 (d, 1H, J = 12.3 Hz), 3.17 (d, 1H, J = 12.4 Hz), 2.90–2.80 (m, 2H), 2.20 (s, 3H), 1.90 (d, 2H, J = 11.2 Hz), 1.78–1.55 (m, 2H) ppm; ^{13}C NMR (101 MHz, DMSO-d_6) δ 165.6, 156.3, 153.3, 141.1, 136.6, 134.1, 131.6, 129., 128.44, 128.3, 127.8, 127.4, 118.7, 112.6, 109.6, 108.4, 107.1, 106.4, 70.5, 55.3, 46.2, 43.5, 42.9, 27.9, 20.5, 10.7 ppm; HRMS calcd. for $C_{26}H_{29}O_4N_4Cl_2$ ([M+H]$^+$): 531.15604, found 531.15457; UHPLC: t_r = 4.167 min (97.3 % at 254 nm).

4.1.41. 3,4-Dichloro-N-(5-methoxy-2-((3-((1-methylpiperidin-3-yl) carbamoyl)benzyl)oxy)phenyl)-5-methyl-1H-pyrrole-2-carboxamide (39)

Compound **38** (0.099 g, 0.174 mmol) was dissolved in methanol. Then triethylamine (72.6 µL, 0.522 mmol) and 37 % water solution of formaldehyde (0.026 g, 0.870 mmol) were added to the reaction mixture. After 1h of stirring, sodium cyanoborohydride (0.0164 g, 0.261 mmol) was added and the mixture was stirred at room temperature overnight. The volatiles were evaporated under reduced pressure. The product was then purified by column chromatography employing DCM/MeOH/NH_4OH = 15/1/0.1 as the mobile phase. Yield: 65 % (0.062 g); white amorphous solid; ^{1}H NMR (400 MHz, DMSO-d_6) δ 12.36 (s, 1H), 9.06 (s, 1H), 8.20 (d, 1H, J = 7.9 Hz), 8.12–8.06 (m, 1H), 8.03 (s, 1H), 7.86 (d, 1H, J = 7.7 Hz), 7.65 (d, 1H, J = 7.5 Hz), 7.50 (t, 1H, J = 7.7 Hz), 7.18 (d, 1H, J = 8.9 Hz), 6.73–6.63 (m, 1H), 5.18 (s, 2H), 3.98–3.87 (m, 1H), 3.73 (s, 3H), 2.84–2.75 (m, 1H), 2.63 (d, 1H, J = 11.1Hz), 2.20 (s, 3H), 2.15 (s, 3H), 1.89–1.72 (m, 3H), 1.67 (d, 1H, J = 13.2 Hz), 1.50 (q, 1H, J = 12.4 Hz), 1.30 (qd, 1H, J = 12.1, 3.9 Hz) ppm; ^{13}C NMR (101 MHz, DMSO-d_6) δ 165.3, 156.3, 153.3, 141.1, 136.5, 134.8, 131.2, 129.5, 128.4, 127.6, 127.3, 118.7, 112.6, 109.7, 108.5, 107.1, 106.4, 70.6, 60.3, 55.4, 55.0, 46.4, 46.0, 29.3, 23.8, 10.8 ppm; HRMS calcd. for $C_{27}H_{31}O_4N_4Cl_2$ ([M+H]$^+$): 545.17169, found 545.17005; UHPLC: t_r = 4.193 min (99.5 % at 254 nm).

4.1.42. 3-((2-Nitrophenoxy)methyl)benzoic acid (40) [26]

The synthesis was performed in accordance with general procedure

D using compound **7** (8.15 g, 28.4 mmol) as starting material. Yield: 81 % (6.30 g); yellow solidified oil; ^{1}H NMR (400 MHz, $CDCl_3$) δ 8.20 (d, J = 1.7 Hz, 1H), 8.12 (dt, J_1 = 7.9 Hz, J_2 = 1.5 Hz, 1H), 7.92 (dd, J_1 = 8.1 Hz, J_2 = 1.8 Hz, 1H), 7.86–7.79 (m, 1H), 7.61–7.51 (m, 2H), 7.16 (dd, J_1 = 8.6 Hz, J_2 = 1.2 Hz, 1H), 7.15–7.06 (m, 1H), 5.33 (s, 2H) ppm; MS (ESI-) m/z = 271.9 $[M-H]^-$.

*4.1.43. tert-Butyl (1-(3-((2-nitrophenoxy)methyl)benzoyl)piperidin-3-yl) carbamate (**41**) [26]*

The synthesis was performed in accordance with general procedure F using compound **40** (0.600 g, 2.20 mmol) as starting material. Yield: 97 % (0.974 g); colorless oil; ^{1}H NMR (400 MHz, $CDCl_3$) δ 7.90 (dd, J_1 = 8.1 Hz, J_2 = 1.7 Hz, 1H), 7.61–7.51 (m, 3H), 7.50–7.40 (m, 2H), 7.15 (dd, J_1 = 8.5 Hz, J_2 = 1.2 Hz, 1H), 7.08 (t, J = 7.7 Hz, 1H), 5.29 (s, 2H), 4.82–4.47 (m, 1H), 4.19–3.96 (m, 1H), 3.85–3.39 (m, 2H), 3.37–3.02 (m, 2H), 2.07 (br s, 1H), 1.89–1.66 (m, 2H), 1.55–1.32 (m, 9H) ppm; MS (ESI+) m/z = 456.0 $[M+H]^+$.

*4.1.44. tert-Butyl 3-(3-((2-nitrophenoxy)methyl)benzamido)piperidine-1-carboxylate (**42**) [26]*

The synthesis was performed in accordance with general procedure F using compound **40** (0.800 g, 2.93 mmol) as starting material. Yield: 79 % (1.33 g); yellow oil; ^{1}H NMR (400 MHz, $CDCl_3$) δ 7.88 (dd, J_1 = 8.6 Hz, J_2 = 2.2 Hz, 2H), 7.74 (dt, J_1 = 7.7 Hz, J_2 = 1.4 Hz, 1H), 7.63 (ddd, J_1 = 7.7 Hz, J_2 = 1.9 Hz, J_3 = 1.0 Hz, 1H), 7.53 (ddd, J_1 = 8.4 Hz, J_2 = 7.4 Hz, J_3 = 1.8 Hz, 1H), 7.47 (t, J = 7.7 Hz, 1H), 7.13 (dd, J_1 = 8.5 Hz, J_2 = 1.1 Hz, 1H), 7.12–7.03 (m, 1H), 5.27 (s, 2H), 4.16 (d, J = 8.7 Hz, 1H), 3.76–3.23 (m, 4H), 1.98–1.68 (m, 3H), 1.44 (s, 9H) ppm, the remaining signal is overlapped with water; MS (ESI+) m/z = 455.7 $[M+H]^+$.

*4.1.45. tert-Butyl (1-(3-((2-aminophenoxy)methyl)benzoyl)piperidin-3-yl) carbamate (**43**) [26]*

The synthesis was performed in accordance with general procedure B using compound **41** (0.800 g, 1.76 mmol) as starting material. The product was further purified by flash column chromatography employing DCM/MeOH = 30/1 as the mobile phase. Yield: 64 % (0.480 g); off-white amorphous solid; ^{1}H NMR (400 MHz, $CDCl_3$) δ 7.52–7.46 (m, 2H), 7.47–7.34 (m, 2H), 6.88–6.77 (m, 2H), 6.78–6.65 (m, 2H), 5.12 (s, 2H), 4.51 (br s, 1H), 4.07–3.57 (m, 4H), 3.53–2.93 (m, 2H), 1.97 (br s, 1H), 1.85–1.59 (m, 2H), 1.41 (s, 9H) ppm; MS (ESI+) m/z = 425.9 $[M+H]^+$.

*4.1.46. tert-Butyl 3-(3-((2-aminophenoxy)methyl)benzamido)piperidine-1-carboxylate (**44**) [26]*

The synthesis was performed in accordance with general procedure B using compound **42** (0.950 g, 2.09 mmol) as starting material. Yield: 90 % (0.802 g); brown oil; ^{1}H NMR (400 MHz, $CDCl_3$) δ 7.85 (s, 1H), 7.71 (d, J = 7.8 Hz, 1H), 7.58 (d, J = 8.1 Hz, 1H), 7.45 (t, J = 7.7 Hz, 1H), 6.88–6.80 (m, 2H), 6.79–6.64 (m, 2H), 5.12 (s, 2H), 4.23–4.14 (m, 1H), 3.85 (br s, 2H), 3.69–3.17 (m, 4H), 1.87 (br s, 1H), 1.69 (br s, 1H), 1.44 (s, 9H) ppm; MS (ESI+) m/z = 425.9 $[M+H]^+$.

*4.1.47. tert-Butyl (1-(3-((2-(3,4-dichlorobenzamido)phenoxy)methyl) benzoyl)piperidin-3-yl)carbamate (**45**)*

The synthesis was performed in accordance with general procedure F using compound **43** (0.240 g, 0.564 mmol) as starting material. Yield: 34 % (0.113 g); colorless oil; ^{1}H NMR (400 MHz, $CDCl_3$) δ 8.59 (s, 1H), 8.49 (dd, J_1 = 7.8 Hz, J_2 = 2.0 Hz, 1H), 7.99 (s, 1H), 7.66 (dd, J_1 = 8.4 Hz, J_2 = 2.1 Hz, 1H), 7.60 (d, J = 8.3 Hz, 1H), 7.58–7.42 (m, 4H), 7.14–7.04 (m, 2H), 7.01 (dd, J_1 = 7.8 Hz, J_2 = 1.7 Hz, 1H), 5.25 (s, 2H), 4.82–4.46 (m, 1H), 4.13–4.00 (m, 1H), 3.84–3.60 (m, 2H), 3.41–2.94 (m, 2H), 1.99 (br s, 1H), 1.87–1.65 (m, 2H), 1.39 (s, 9H) ppm; MS (ESI-) m/z = 596.3 $[M-H]^-$.

*4.1.48. tert-Butyl 3-(3-((2-(3,4-dichlorobenzamido)phenoxy)methyl) benzamido)piperidine-1-carboxylate (**46**)*

The synthesis was performed in accordance with general procedure F using compound **44** (0.350 g, 0.822 mmol) as starting material. Yield: 49 % (0.243 g); off-white amorphous solid; ^{1}H NMR (400 MHz, DMSO-d_6) δ 9.85 (s, 1H), 8.24 (d, J = 7.0 Hz, 1H), 8.14 (d, J = 2.2 Hz, 1H), 7.98 (s, 1H), 7.92 (dd, J_1 = 8.3 Hz, J_2 = 2.1 Hz, 1H), 7.78 (dd, J_1 = 10.8 Hz, J_2 = 8.0 Hz, 2H), 7.64 (ddd, J_1 = 7.7 Hz, J_2 = 4.5 Hz, J_3 = 1.7 Hz, 2H), 7.45 (t, J = 7.6 Hz, 1H), 7.26–7.13 (m, 2H), 7.00 (td, J_1 = 7.4 Hz, J_2 = 1.6 Hz, 1H), 5.24 (s, 2H), 4.09–3.70 (m, 3H), 2.76 (t, J = 10.9 Hz, 1H), 1.88–1.81 (m, 1H), 1.75–1.68 (m, 1H), 1.53–1.30 (m, 12H) ppm; MS (ESI+) m/z = 597.8 $[M+H]^+$.

*4.1.49. 1-(3-((2-(3,4-Dichlorobenzamido)phenoxy)methyl)benzoyl) piperidin-3-aminium chloride (**47**)*

The synthesis was performed in accordance with general procedure G using compound **45** (0.089 g, 0.149 mmol) as starting material. The product was further purified by flash column chromatography employing DCM/MeOH/NH_4OH = 10/1/0.1 as the mobile phase. After evaporation of the joint fractions of the clean product, the residue was taken up into methanol and the product was transformed into salt form by adding 4 M HCl in dioxane to the mixture (3 equiv.). The solvent was then evaporated under reduced pressure to give compound **47**. Yield: 68 % (0.054 g); white amorphous solid; ^{1}H NMR (400 MHz, $CDCl_3$) δ 8.57 (br s, 4H), 8.28 (d, J = 7.3 Hz, 1H), 7.87 (s, 1H), 7.70–7.31 (m, 6H), 7.03–6.87 (m, 3H), 5.11 (s, 2H), 4.00–3.84 (m, 1H), 3.61–3.06 (m, 4H), 2.17–1.67 (m, 3H), 1.46–1.30 (m, 1H) ppm; ^{13}C NMR (101 MHz, DMSO-d_6) δ 169.4, 163.1, 151.6, 137.5, 135.8, 134.9, 134.4, 131.4, 130.9, 129.6, 128.5, 128.3, 127.9, 126.8, 126.6, 126.3, 126.1, 125.6, 120.7, 113.3, 69.2, 46.2, 43.9, 28.0, 22.5, 12.4 ppm; HRMS calcd. for $C_{26}H_{26}O_3N_3Cl_2$ ($[M+H]^+$): 498.13457, found 498.13433; UHPLC: t_r = 4.187 min (96.8 % at 254 nm).

*4.1.50. 3-(3-((2-(3,4-Dichlorobenzamido)phenoxy)methyl)benzamido) piperidin-1-ium chloride (**48**)*

The synthesis was performed in accordance with general procedure H using compound **46** (0.227 g, 0.379 mmol) as starting material. The product was further purified by flash column chromatography employing DCM/MeOH/NH_4OH = 9/1/0.1 as the mobile phase. After evaporation of the joint fractions of the clean product the residue was taken up into methanol and the product was transformed into salt form by adding 4 M HCl in dioxane to the mixture (3 equiv.). The solvent was then evaporated under reduced pressure to give compound **48**. Yield: 78 % (0.158 g); white amorphous solid; ^{1}H NMR (400 MHz, DMSO-d_6) δ 9.92 (s, 1H), 9.32–9.26 (m, 1H), 9.04–8.98 (m, 1H), 8.67 (d, J = 7.7 Hz, 1H), 8.18 (d, J = 2.1 Hz, 1H), 8.09 (t, J = 1.8 Hz, 1H), 7.95 (dd, J_1 = 8.3 Hz, J_2 = 2.1 Hz, 1H), 7.86 (dt, J_1 = 7.8 Hz, J_2 = 1.3 Hz, 1H), 7.80 (d, J = 8.3 Hz, 1H), 7.72–7.58 (m, 2H), 7.46 (t, J = 7.7 Hz, 1H), 7.26–7.13 (m, 2H), 7.00 (td, J_1 = 7.3 Hz, J_2 = 1.5 Hz, 1H), 5.24 (s, 2H), 4.30–4.13 (m, 1H), 3.32–3.25 (m, 1H), 3.21–3.11 (m, 1H), 2.95–2.78 (m, 2H), 1.94–1.83 (m, 2H), 1.78–1.54 (m, 2H) ppm; ^{13}C NMR (101 MHz, DMSO-d_6) δ 165.7, 163.1, 151.4, 137.3, 135.0, 134.3, 134.2, 131.3, 130.8, 130.1, 129.7, 128.3, 127.9, 126.8, 126.6, 126.6, 126.4, 125.9, 120.6, 113.2, 69.4, 46.1, 43.4, 42.9, 27.9, 20.3 ppm; HRMS calcd. for $C_{26}H_{26}O_3N_3Cl_2$ ($[M+H]^+$): 498.13457, found 498.13435; UHPLC: t_r = 4.263 min (100 % at 254 nm).

*4.1.51. 3,4-Dichloro-N-(2-((3-((1-methylpiperidin-3-yl)carbamoyl) benzyl)oxy)phenyl)benzamide (**49**)*

Compound **48** (0.050 g, 0.093 mmol) was dissolved in methanol. Then triethylamine (25.9 μL, 0.187 mmol) and 37 % water solution of formaldehyde (35.1 μL, 0.467 mmol) were added to the reaction mixture. After 1h of stirring, sodium cyanoborohydride (0.012 g, 0.187 mmol) was added and the mixture was stirred at room temperature overnight. The volatiles were evaporated under reduced pressure. The product was then purified by column chromatography employing DCM/

MeOH/NH_4OH = 9/1/0.1 as the mobile phase. Yield: 75 % (0.036 g); white amorphous solid; ^{1}H NMR (400 MHz, DMSO-d_6) δ 9.86 (s, 1H), 8.17–8.10 (m, 2H), 7.99 (t, J = 1.8 Hz, 1H), 7.92 (dd, J_1 = 8.3 Hz, J_2 = 2.1Hz, 1H), 7.83–7.73 (m, 2H), 7.68–7.60 (m, 2H), 7.45 (t, J = 7.7 Hz, 1H), 7.27–7.14 (m, 2H), 7.05–6.97 (m, 1H), 5.24 (s, 2H), 3.98–3.85 (m, 1H), 2.82–2.75 (m, 1H), 2.68–2.61 (m, 1H), 2.17 (s, 3H), 1.89–1.63 (m, 4H), 1.58–1.44 (m, 1H), 1.33–1.19 (m, 1H) ppm; ^{13}C NMR (101 MHz, DMSO-d_6) δ 165.5, 163.1, 151.3, 137.3, 135.0, 134.8, 134.3, 131.4, 130.8, 129.7, 129.6, 128.2, 127.8, 126.7, 126.7, 126.6, 126.1, 125.7, 120.7, 113.2, 69.4, 60.2, 55.0, 46.3, 46.0, 29.2, 23.8 ppm; HRMS calcd. for $C_{27}H_{28}O_3N_3Cl_2$ ([M+H]$^+$): 512.15022, found 512.15018; UHPLC: t_r = 4.310 min (100 % at 254 nm).

4.2. Pharmacophore screening

For each compound in the in-house library of TopoIIα inhibitors, including compounds **1**–**3** (Fig. 1), a conformer library was generated using iCon algorithm in LigandScout Expert 4.5 with the default "BEST" settings. Maximum number of conformers per molecules was set to 200, Timeout (s) was 600, RMS threshold was 0.8, energy window was 20.0, maximum pool size was 4,000, and maximum fragment build time was 30. TopoIIα inhibitor library was saved in the LDB format using default settings of the idbgen algorithm.

The ligand-based pharmacophore models for identification of Hsp90β C-terminal domain inhibitors [28] was used to query the library of TopoIIα inhibitors in LDB format. Pharmacophore-Fit was used as a scoring function, Match all query features was used as a screening mode, Stop after first matching conformation was set as retrieval mode, the Max. number of omitted features was set to 0, and Check exclusion volumes was set to true. Pharmacophore fit score was used to rank the hits of the pharmacophore screening.

4.3. Molecular docking simulations

Molecular docking calculations were performed using Schrödinger Release 2022-1 (Schrödinger, LLC, New York, NY, USA, 2022). The cryoEM structure of Hsp90β (PDB entry: 5FWK [38]) and X-ray crystal structure of the human topoisomerase IIα (PDB entry: 4R1F [37]) in complex with ligands were prepared using Protein Preparation Wizard with the default settings: bond orders were assigned using CCD database, missing hydrogens were added, termini were capped, the missing side chains were modelled with Prime, and het protonation states (pH 7.0 ± 2.0) were modeled with Epik [54]. The receptor grids were calculated for the ligand-binding sites. In the case of Hsp90β, all waters and cosolvents were deleted. In the case of TopoIIα, all crystal waters and cosolvents were deleted, and Asn102 carboxamide group was defined as hydrogen bond acceptor and donor constraint. Ligand structures were prepared using LigPrep module and ionized with Epik at pH = 7.4 using OPLS4 force field. The compounds were then docked using the Glide XP protocol as implemented in Schrödinger Release 2022-1 (Glide, Schrödinger, LLC, New York, NY, USA, 2022). The highest scored docking conformation was used for analysis and presentation.

4.4. Molecular dynamics simulations

Hsp90β or TopoIIα in docking complex with inhibitor **(*R*)-3** was used as an input for molecular dynamics simulation using Desmond [55]. The structures of the docking complexes were prepared with System Builder. The TIP4P water molecules up to 10 Å from the protein surface were added to solvate the system in an orthorhombic box. Solvated system was then neutralized by adding sodium and chloride ions at a concentration of 0.15 M. OPLS_2005 force field [56] was used for parametrization of the protein–ligand complex. Default Desmond relaxation protocol was used for the equilibration stage: (1) 100 ps of Brownian dynamics NVT, 10 K, small timesteps, with restraints on the solute heavy atoms, (2) 12 ps NVT, 10 K, with small timesteps and restraints on the solute heavy atoms, (3) 12 ps NPT, 10 K, and restraints on the solute heavy atoms, (4) 24 ps unrestrained NPT. The equilibration was followed by the 200 ns long production stage: NPT ensemble at 300 K and 1.013 bar pressure with Langevin thermostat and barostat (1 and 2 ps relaxation time, respectively), RESPA integrator with 2 fs time step, cut-off scheme at 9.0 Å. Molecular dynamics trajectory was analyzed using Simulation Interactions Diagram algorithm in Maestro.

4.5. Hsp90α and Hsp90β affinity determination by fluorescence-based thermal shift assay

To assess the binding of known TopoIIα inhibitors to the Hsp90β-NTD and Hsp90α-NTD, a fluorescence-based thermal shift assay (FTSA) was used [33]. In this assay, the thermal stability of both free protein and ligand-bound protein were evaluated. To conduct the experiments, a Rotor-Gene Q 6-Plex spectrofluorometer was used, with excitation at 365 nm and detection at 460 nm. Solutions encompassed 10 μM of protein, while the concentrations of the evaluated ligands were varied in the ranges from 0 to 200 μM. These solutions were then heated from 25 °C to 80 °C at a constant rate of 1 °C/min. Protein unfolding was monitored using the fluorescent dye 8-anilino-1-naphthalenesulfonate at a concentration of 100 μM. The buffer, in which the experiments were performed, contained 50 mM sodium phosphate, 100 mM sodium chloride, 2 % DMSO, and the pH of the buffer was 7.5. Melting curves (T_m values) were fitted using Thermott [57].

4.6. Topoisomerase IIα decatenation assay

Initially the activity of the enzyme (TopoIIα) was evaluated before the compounds were tested [26]. 1 unit (U) was defined as the required amount of the enzyme to completely release minicircles from 200 ng of kDNA by full decatenation. This was first used to determine the activity of a known TopoIIα inhibitor etoposide. The experiments with test compound and etoposide were performed in duplicate. Both in the etoposide activity determination and in compound testing, the final DMSO concentration was 1 %. Compounds were added to the reaction before the addition of the enzyme and tested at 10 μM and 100 μM concentrations.

1 U of human topoisomerase IIα was incubated with 200 ng of kDNA in a 30 μL reaction at 37 °C for 30 min. The conditions were as follows: 50 mM Tris×HCl (pH7.5), 125 mM NaCl, 10 mM $MgCl_2$, 5 mM DTT and 100 μg/mL albumin. To stop the reactions 30 μL chloroform/isoamyl alcohol (24:1) was added along with 30 μL of Stop dye which comprised 40 % sucrose (w/v), 10 mM EDTA, 0.5 μg/mL bromophenol blue and 100 mM Tris×HCl (pH 7.5). Next, the prepared samples were loaded on a 1.0 % TAE gel run. The samples were run at 90 V for ~1 h

Bands were visualized by ethidium staining for 10 min, de-stained for 10 min in water and analyzed by gel documentation equipment (Syngene, Cambridge, UK) and quantitated using Syngene Gene Tools software. Raw gel data (fluorescent band volumes) collected from Syngene, GeneTools gel analysis software was calculated as a % of the 100 % control (the fully decatenated DNA band) and converted to % activity with addition of the test compound. Fluorescence exceeding 100 % of decatenation were normalized to 100 %.

4.7. Hsp90 CTD inhibition TR-FRET assay

The TR-FRET kit used to evaluate binding to the CTD of Hsp90β was obtained from BPS Bioscience (San Diego, CA, USA) [33]. The kit is used to measure the protein–protein interaction between cyclophilin D (Hsp90 co-chaperone) and Hsp90 CTD, as this interaction can be disrupted by inhibitors of the CTD of Hsp90. The assay followed the manufacturer's protocol as outlined below. The reaction included a terbium-labelled donor, a dye-labelled acceptor, the CTD of Hsp90β, PPID, and newly prepared compounds. As a control compound,

novobiocin, a known inhibitor of the Hsp90 CTD, was employed. In the positive control experiment, the inhibitor solution was replaced by DMSO to achieve the same 1 % final DMSO concentration. Meanwhile, in the negative control wells, assay buffer was added instead of cyclophilin D. The assay was carried out in duplicates for both samples and controls. Upon the addition of all, the solutions were incubated for 2 h at ambient temperature. Afterwards, a time-resolved fluorescence resonance energy transfer (TR-FRET) was measured using a Tecan Spark Multimode Microplate reader (Tecan Trading AG, Switzerland). The obtained measurements were used in the calculation of the results, which are presented herein as percentages of residual C-terminal Hsp90β CTD activity. The equation used in the calculations was as follows: $\%\text{Activity} = 100 \times (\text{FRET}_{\text{sample}} - \text{FRET}_{\text{negative control}}) / (\text{FRET}_{\text{positive control}} - \text{FRET}_{\text{negative control}})$. The FRET value in this formula represents the ratio between dye-acceptor emission and Tb-donor emission.

4.8. Ligand-observed protein NMR studies

High-resolution NMR spectra were acquired using a Bruker Avance Neo 600 MHz spectrometer equipped with a cryoprobe at 25 °C. The data collection was performed using pulse sequences from the Bruker pulse program library, and the analysis was carried out by Bruker Topspin 4.2.0 software. To supress the residual water signal, excitation sculpting [58] with a 5 ms selective pulse was used, along with a $T_1\rho$ filter of 100 ms to eliminate background protein resonances. The ^{1}H spectral width was set to 5882 Hz. NMR samples were prepared in a buffer containing 50 mM potassium phosphate (pD 7.5), 100 mM KCl in D_2O, with 5 mM $MgSO_4$, 2 mM DTT-d_{10}, 0.02 % NaN_3 and 5 % DMSO-d_6. Proton assignment (Fig. S5 and Table S1) was achieved by combining TOCSY, NOESY, and HSQC spectra. The ^{1}H STD and trNOESY spectra, a protein:ligand ratio of 1:100 was used, with final concentrations of 2 μM for the protein and 0.2 mM for the ligand [33].

In the ^{1}H STD ligand epitope mapping experiments [59], 65 536 data points were recorded (5.57 s acquisition time) with a relaxation delay of 1.63 s and 5,840 scans. A short protein saturation time of 0.5 s was applied to reduce the relaxation effects on the STD amplification factors [60]. T_1 inversion-recovery experiments showed that the ^{1}H T_1 relaxation times for ligand protons with detectable STD signals ranged from 1.3 s to 4.2 s (Table S2). Selective on-resonance saturation of Hsp90β was applied at −0.827 ppm, with the transmitter offset referenced to 4.70 ppm. Off-resonance irradiation for the reference spectrum was set at 30 ppm. The spectra were zero-filled and apodized using an exponential line-broadening function of 3 Hz. The errors in the STD amplification factors were calculated using the following formula [61]:

$$\text{STD amplification factor absolute error} = \text{STD amplification factor} \times \left[\left(\frac{N_{STD}}{I_{STD}} \right)^2 + \left(\frac{N_{REF}}{I_{REF}} \right)^2 \right]^{\frac{1}{2}}$$

N_{STD} and N_{REF} are the noise levels in STD and reference spectra. I_{STD} and I_{REF} are the signal intensities in STD and reference spectra. The maximum relative error for the STD amplification factors was 5.1 % (Table S2).

For the trNOESY [62] spectra, 4,096 data points were recorded in t_2, 64 scans, 256 complex points in t_1, a mixing time of 350 ms, and a relaxation delay of 1.5 s. The spectra were apodized with a squared sine bell function shifted by π/2 in both dimensions.

4.9. Cell culture

The Ewing sarcoma cell line SK-N-MC (a kind gift from Beat Schäfer) was cultured as a monolayer and maintained in RPMI 1640 medium. The medium used was further supplemented with 10 % heat-inactivated fetal bovine serum, 100 μg/mL streptomycin, 100 U/mL penicillin, and 2 mM L-glutamine. Both medium and its components were acquired from Sigma-Aldrich (St. Louis, MO, USA). The atmosphere in which the cells were grown was humidified and it contained 5 % CO_2 at 37 °C.

4.10. MTS assay

The antiproliferative activities of the compounds against the Ewing sarcoma cell line SK-N-MC were evaluated using an MTS assay (Promega, Madison, WI, USA) following the manufacturer's instructions [32]. The seeding density for the cells in 96-well plates was 2000 cells/well. After a 24-h incubation period, the cells were treated with the final compounds or vehicle control (0.5 % DMSO), with novobiocin serving as the positive control. Following a 72-h incubation, 10 μL of CellTiter96 Aqueous One Solution Reagent acquired from Promega (Madison, WI, USA), was added to each individual well. The cells were then additionally incubated for 3 h. Absorbance was then measured using a microplate reader (Synergy 4 Hybrid; BioTek, Winooski, VT, USA). Each independent experiment was conducted twice, each time performed in triplicate. The IC_{50} values, representing the concentration at which a compound produced a half-maximal response, were determined using GraphPad Prism 10.0 software (San Diego, CA, USA) and are reported as means from the independent measurements.

4.11. Apoptosis evaluation

To evaluate the induction of apoptosis of SK-N-MC cells, phosphatidylserines were detected employing an R-phycoerythrin (R-PE)–Annexin V conjugate and nucleic acids in dead cells were identified by Sytox Blue Dead Cell Stain [43]. Both reagents were purchased at Invitrogen (Carlsbad, CA, USA), and the assay was performed following the manufacturer's instructions. In brief, SK-N-MC cells were seeded in a six-well plate at a density of 2.5×10^5/well. After 24 h, the cells were washed with PBS and then exposed to with 0.375 μM, 1.5 μM, or 7 μM of compound **3** for 24–72 h. Afterwards, the medium containing detached cells was collected. Then the attached cells were harvested and combined with the previously collected cells from the medium. The combined cells were washed twice with cold PBS, and then resuspended in 100 μL of annexin-binding buffer (Invitrogen, Carlsbad, CA, USA), which contained 2.5 μL R-PE–Annexin V solution and 750 nM Sytox Blue. The mixture was then incubated in the dark for 15 min at ambient temperature. Prior to measurement, additional 200 μL of annexin-binding buffer was added. A minimum of 10,000 events were collected using a flow cytometer (Attune NxT; Invitrogen, Carlsbad, CA, USA). The cell populations were identified as follows: viable cells not undergoing apoptosis were visible as Annexin V (ANV)-/Sytox Blue (SB)-, early apoptotic or proapoptotic cells were visible as ANV+/SB−, late apoptotic cells were visible as ANV+/SB+, and indicates necrotic cells were visible as ANV−/SB+.

4.12. Cell cycle evaluation

In evaluation of cell cycle propidium iodide (PI), acquired form Sigma-Aldrich (St. Louis, MO, USA), was used [43]. SK-N-MC cells were seeded in a six-well plate at a density of 2.5×10^5/well. After 24 h, the cells were washed with PBS and treated with 0.70 and 1.5 μM of compound **3** for 24–48 h. The medium containing detached cells was collected first. Then, the attached cells were harvested and both fractions of cells were combined. Merged cells were first washed twice with PBS. Next, the cells were incubated with ice-cold 85 % ethanol for 15 min at −20 °C and were thus fixed and permeabilized. Then, they were rehydrated with PBS at ambient temperature. This was followed by incubation of the cells in the dark for 15 min at ambient temperature in 500 μL of PI-binding buffer which contained 1 μM PI and 1 mg/mL Ribonuclease A (Qiagen, Hilden, Germany). In the measurement a minimum of 10,000 events were collected using a flow cytometer (Attune NxT; Invitrogen, Carlsbad, CA, USA).

4.13. Western blot

Cells were seeded at a density of 750,00 per well in a six-well plate. After 24 h, the media was removed, and the cells were treated with 1 μM and 5 μM concentrations of compound **3**, dissolved in the growth medium, along with a negative control (0.5 % DMSO solution in the growth medium). Following a 24-h incubation, the medium was collected along with the detached cells. The remaining cells were washed with PBS (Gibco, Thermo Fisher Scientific, Waltham, MA, USA), and the detached cells in the PBS were merged with the centrifuged cells from the medium. Both attached and detached cells were then lysed together using RIPA buffer (50 mM Tris-HCl pH 7.4, 150 mM NaCl, 1 % NP-40, 0.5 % sodium deoxycholate, 1 mM EDTA) containing protease (1:100 Halt™ Protease Inhibitor Cocktail, Thermo Fisher Scientific, Waltham, MA, USA) and phosphatase (1:100 Halt™ Phosphatase Inhibitor Cocktail, Thermo Fisher Scientific, Waltham, MA, USA) inhibitors. Next, protein lysates were frozen to −80 °C for 24 h, then thawed, sonicated, and centrifuged at 15,000 rpm for 20 min at 4 °C. The supernatants were then collected and the protein concentration in the lysates was determined by commercially available DC protein assay (Bio-Rad, Hercules, California, USA). 20 μg of isolated proteins were then separated using SDS-PAGE (7.5 % acrylamide/bisacrylamide gel). For electrophoresis, 80 V was applied for the first 15 min, followed by 130 V for the final 60 min. Following the separation, iBlot 3 Dry Blotting System (Thermo Fisher Scientific, Waltham, MA, USA) was used for a transfer onto a PVDF membrane. The membranes were first incubated in 5 % BSA for 1 h at room temperature in order to block nonspecific binding sites. The primary antibodies used in the detection of proteins included anti-Hsp90 Rabbit mAb (1:1000), anti-Hsp70 Mouse mAb (1:1000), anti-c-Raf Rabbit mAb (1:1000) and anti-β-tubulin Rabbit mAb (1:1000), all purchased from Cell Signaling (Danvers, MA, USA). Prior to detection, incubation with secondary antibodies was performed at ambient temperature using either anti-rabbit IgG, HRP-linked antibody (1:10000) or anti-mouse IgG, Hrp-linked antibody (1:10000) depending on the primary antibody type. The membranes were washed, and SuperSignal™ West Femto Maximum Sensitivity Substrate (Thermo Fisher Scientific, Waltham, MA, USA) was added and UVITEC Cambridge Imaging System (UVITEC, Cambridge, UK) was used to visualize the proteins. Western blot bands were quantified by densitometric analysis using NineAlliance software, and relative densities were calculated in relation to β-tubulin which was used as the loading control.

4.14. In vivo efficacy study in zebrafish larvae

Zebrafish embryos from mitfa$^{b692/b692}$; ednrba$^{b140/b140}$ strains were raised for transplantation until 2 days post-fertilization (dpf) at 28 °C, dechorionated, and anesthetized using 1× Tricaine (0.16 g/L Tricaine, Sigma-Aldrich Chemie GmbH, Germany, Cat No. E1052110G, adjusted to pH 7 with 1 M Tris pH 9.5 in E3). Upon anesthetization and prior to transplantation the larvae were placed on a petri dish lid, which was coated with solidified 2 % agarose, as previously described [53]. For tumor cell injection, borosilicate glass capillaries (GB100T-8P, without filament, Science Products GmbH, Germany) were pulled with a needle puller (P-97, Sutter Instruments, USA). Ewing sarcoma cells were harvested and a cell suspension in PBS was prepared with a final concentration of 100 cells/nL. Approximately 5 μL of thus prepared tumor cell suspension was loaded into the needles. The needles were then attached to a micromanipulator (M3301R, World Precision Instruments Inc., Germany). The prepared setup was connected to a microinjector (FemtoJet 4i, Eppendorf, Germany). Next, Ewing sarcoma cell suspension was injected in the perivitelline space (PVS) of the zebrafish larvae. Two hours after the injection, the xenotransplanted larvae were screened to identify those displaying exclusively tumor cells in the PVS. The suitable larvae were then maintained at 34 °C.

To perform automated imaging, the larvae were again anesthetized using 1× Tricaine after 1 day post injection (1 dpi) and placed in a 96-well ZF plate (Hashimoto Electronic Industry Co, Japan). The plate contained 0.5 % ultra-low gelling agarose (Sigma-Aldrich Chemie GmbH, Germany, Cat. No. A2576-25G). Operetta CLS high-content imager (Revvity, USA) with a 5× air objective was used for image acquisition. Images were acquired in brightfield (40 ms and 10 % intensity) and fluorescence for GFP (excitation: 460–490 nm at 100 %, emission: 500–550 nm for 400 ms). Per field a total of 21 planes with a 25 μm spacing were imaged. Afterwards, the larvae were removed from the plate used for imaging and they were placed into the corresponding multi-well plate well. A freshly prepared compound/solvent master mix in E3 was then added to achieve a final concentration of 10 μM of compound **3**/1 % DMSO, 30 μM 17-DMAG/1 % DMSO as the positive control, or DMSO (1 %) as the negative control. The larvae were then incubated with these mixtures for two days (until 3 dpi), and then new images were collected. The experiment was carried out 3 times in the same fashion. Harmony Software 4.9 (Revvity, USA) was employed to quantify the tumor size. The footprint area of the tumor was projected along the z-axis onto the x-y plane selected for further analysis. The relative change in tumor size was calculated as the footprint area at 3 dpi divided by the area at 1 dpi.

CRediT authorship contribution statement

Jaka Dernovšek: Writing – review & editing, Writing – original draft, Visualization, Methodology, Investigation, Formal analysis. **Dunja Urbančič:** Writing – review & editing, Writing – original draft, Visualization, Methodology, Investigation, Formal analysis. **Živa Zajec:** Writing – review & editing, Methodology, Investigation. **Caterina Sturtzel:** Writing – review & editing, Visualization, Methodology, Investigation. **Sarah Grissenberger:** Writing – review & editing, Methodology, Investigation. **Andrea Wenninger-Weinzierl:** Writing – review & editing, Methodology, Investigation. **Marius Gedgaudas:** Writing – review & editing, Visualization, Methodology, Investigation. **Asta Zubrienė:** Writing – review & editing, Supervision, Methodology. **Tjaša Goričan:** Investigation, Methodology, Visualization, Writing – review & editing. **Simona Golič Grdadolnik:** Funding acquisition, Methodology, Supervision, Writing – review & editing. **Žiga Skok:** Writing – review & editing, Methodology, Investigation. **Janez Ilaš:** Writing – review & editing, Supervision, Methodology. **Martin Distel:** Writing – review & editing, Supervision, Methodology, Funding acquisition, Formal analysis. **Nace Zidar:** Writing – review & editing, Supervision, Methodology, Conceptualization. **Tihomir Tomašič:** Writing – review & editing, Writing – original draft, Visualization, Supervision, Methodology, Investigation, Funding acquisition, Formal analysis, Conceptualization.

Declaration of competing interest

The authors declare that they have no known competing financial interests or personal relationships that could have appeared to influence the work reported in this paper.

Data availability

Data will be made available on request.

Acknowledgements

This work was supported by the Slovenian Research Agency (Grant Nos. P1-0208, P1-0010, J1-1717, J1-4400, BI-AT/23-24-008, J1-50038 (HSP90IES), the BMBWF through OeAD grant SI 29/2023, Austrian Research Promotion Agency (FFG) project 7940628 (Danio4Can) and Austrian Science Fund (FWF) project I6685-B (HSP90IES) (M.D.). Ema Sopčič is acknowledged for her contributions in the synthetic part of the work and Maja Frelih is acknowledged for acquisition of HRMS spectra.

Appendix A. Supplementary material

Supplementary data to this article can be found online at https://doi.org/10.1016/j.bioorg.2024.107850.

References

[1] F. Bray, M. Laversanne, H. Sung, J. Ferlay, R.L. Siegel, I. Soerjomataram, A. Jemal, Global Cancer Statistics 2022: GLOBOCAN estimates of incidence and mortality worldwide for 36 cancers in 185 countries, CA Cancer J. Clin. 74 (3) (2024) 229–263, https://doi.org/10.3322/caac.21834.

[2] Main cause of death for people under 65 years: cancer - Eurostat. https://ec.europa.eu/eurostat/web/products-eurostat-news/w/ddn-20240507-1 (accessed 2024-06-07).

[3] N.M. Ayoub, Editorial: Novel combination therapies for the treatment of solid cancers, Front. Oncol. 11 (2021).

[4] R.B. Mokhtari, T.S. Homayouni, N. Baluch, E. Morgatskaya, S. Kumar, B. Das, H. Yeger, Combination therapy in combating cancer, Oncotarget 8 (23) (2017) 38022–38043. 10.18632/oncotarget.16723.

[5] O.V. Ancker, M. Krüger, M. Wehland, M. Infanger, D. Grimm, Multikinase inhibitor treatment in thyroid cancer, Int. J. Mol. Sci. 21 (1) (2019) 10, https://doi.org/10.3390/ijms21010010.

[6] C.C. Ayala-Aguilera, T. Valero, Á. Lorente-Macías, D.J. Baillache, S. Croke, A. Unciti-Broceta, Small molecule kinase inhibitor drugs (1995–2021): medical indication, pharmacology, and synthesis, J. Med. Chem. 65 (2) (2022) 1047–1131, https://doi.org/10.1021/acs.jmedchem.1c00963.

[7] R. Dutta, M. Inouye, GHKL, an emergent ATPase/kinase superfamily, Trends Biochem. Sci. 25 (1) (2000) 24–28, https://doi.org/10.1016/S0968-0004(99)01503-0.

[8] J.L. Delgado, C.-M. Hsieh, N.-L. Chan, H. Hiasa, Topoisomerases as anticancer targets, Biochem. J. 475 (2) (2018) 373–398, https://doi.org/10.1042/BCJ20160583.

[9] A.M. Jaeger, L. Whitesell, HSP90: enabler of cancer adaptation, Annu. Rev. Cancer Biol. 3 (1) (2019) 275–297, https://doi.org/10.1146/annurev-cancerbio-030518-055533.

[10] A. Hoter, M.E. El-Sabban, H.Y. Naim, The HSP90 family: structure, regulation, function, and implications in health and disease, Int. J. Mol. Sci. 19 (9) (2018) 2560, https://doi.org/10.3390/ijms19092560.

[11] B. Birbo, E.E. Madu, C.O. Madu, A. Jain, Y. Lu, Role of HSP90 in cancer, Int. J. Mol. Sci. 22 (19) (2021) 10317, https://doi.org/10.3390/ijms221910317.

[12] J.J. Champoux, DNA topoisomerases: structure, function, and mechanism, Annu. Rev. Biochem. 70 (1) (2001) 369–413, https://doi.org/10.1146/annurev.biochem.70.1.369.

[13] A.K. McClendon, N. Osheroff, DNA topoisomerase II, genotoxicity, and cancer, Mutat. Res. 623 (1–2) (2007) 83–97, https://doi.org/10.1016/j.mrfmmm.2007.06.009.

[14] K.R. Vann, A.A. Oviatt, N. Osheroff, Topoisomerase II poisons: converting essential enzymes into molecular scissors, Biochemistry 60 (21) (2021) 1630–1641, https://doi.org/10.1021/acs.biochem.1c00240.

[15] Ž. Skok, N. Zidar, D. Kikelj, J. Ilaš, Dual inhibitors of human DNA topoisomerase II and other cancer-related targets, J. Med. Chem. 63 (3) (2020) 884–904, https://doi.org/10.1021/acs.jmedchem.9b00726.

[16] S.M. Hoy, Pimitespib: first approval, Drugs 82 (13) (2022) 1413–1418, https://doi.org/10.1007/s40265-022-01764-6.

[17] K.-Y. Jun, Y. Kwon, Proposal of dual inhibitor targeting ATPase domains of topoisomerase II and heat shock protein 90, Biomol. Ther. 24 (5) (2016) 453–468, https://doi.org/10.4062/biomolther.2016.168.

[18] X. Pan, T. Mao, Y. Mai, C. Liang, W. Huang, Y. Rao, Z. Huang, S. Huang, Discovery of quinacrine as a potent Topo II and Hsp90 dual-target inhibitor, repurposing for cancer therapy, Molecules 27 (17) (2022) 5561, https://doi.org/10.3390/molecules27175561.

[19] S. El-Kalyoubi, S.A. El-Sebaey, A.M. Rashad, H.A. AL-Ghulikah, M.M. Ghorab, S. M. Elfeky, Synthesis, DFT calculations, and anti-proliferative evaluation of pyrimidine and selenadiazolopyrimidine derivatives as dual topoisomerase II and HSP90 inhibitors, J. Enzyme Inhib. Med. Chem. 38 (1) (2023) 2198163, https://doi.org/10.1080/14756366.2023.2198163.

[20] X. Xie, N. Zhang, X. Li, H. Huang, C. Peng, W. Huang, L.J. Foster, G. He, B. Han, Small-molecule dual inhibitors targeting heat shock protein 90 for cancer targeted therapy, Bioorg. Chem. 139 (2023) 106721, https://doi.org/10.1016/j.bioorg.2023.106721.

[21] Z.-N. Li, Y. Luo, HSP90 inhibitors and cancer: prospects for use in targeted therapies (review), Oncol. Rep. 49 (1) (2023) 1–13, https://doi.org/10.3892/or.2022.8443.

[22] J. Sanchez, T.R. Carter, M.S. Cohen, B.S. Blagg, Old and new approaches to target the hsp90 chaperone, Curr. Cancer Drug Targets 20 (4) (2020) 253–270, https://doi.org/10.2174/1568009619666191202101330.

[23] S. Maiti, K. Bhattacharya, D. Wider, D. Hany, O. Panasenko, L. Bernasconi, N. Hulo, D. Picard, Hsf1 and the molecular chaperone Hsp90 support a "Rewiring Stress Response" leading to an adaptive cell size increase in chronic stress, Elife 12 (2023), https://doi.org/10.7554/eLife.88658.2.

[24] E. Amatya, B.S.J. Blagg, Recent advances toward the development of Hsp90 C-terminal inhibitors, Bioorg. Med. Chem. Lett. 80 (2023) 129111, https://doi.org/10.1016/j.bmcl.2022.129111.

[25] Ž. Skok, M. Durcik, D. Gramec Skledar, M. Barančoková, L. Peterlin Mašič, T. Tomašič, A. Zega, D. Kikelj, N. Zidar, J. Ilaš, Discovery of new ATP-competitive inhibitors of human DNA topoisomerase iiα through screening of bacterial topoisomerase inhibitors, Bioorg. Chem. 102 (2020) 104049, https://doi.org/10.1016/j.bioorg.2020.104049.

[26] Ž. Skok, M. Durcik, Ž. Zajec, D. Gramec Skledar, K. Bozovičar, A. Pišlar, T. Tomašič, A. Zega, L. Peterlin Mašič, D. Kikelj, N. Zidar, J. Ilaš, ATP-competitive inhibitors of human DNA topoisomerase IIα with improved antiproliferative activity based on N-phenylpyrrolamide scaffold, Eur. J. Med. Chem. 249 (2023) 115116, https://doi.org/10.1016/j.ejmech.2023.115116.

[27] J. Dernovšek, T. Goričan, M. Gedgaudas, Ž. Zajec, D. Urbančič, A. Jug, Ž. Skok, C. Sturtzel, M. Distel, S. Golič Grdadolnik, K. Babu, A. Panchamatia, T. R. Stachowski, M. Fischer, J. Ilaš, A. Zubrienė, D. Matulis, N. Zidar, T. Tomašič, Hiding in plain sight: optimizing topoisomerase iiα inhibitors into Hsp90β selective binders, Eur. J. Med. Chem. 116934 (2024), https://doi.org/10.1016/j.ejmech.2024.116934.

[28] T. Tomašič, M. Durcik, B.M. Keegan, D.G. Skledar, Ž. Zajec, B.S.J. Blagg, S. D. Bryant, Discovery of novel Hsp90 C-terminal inhibitors using 3D-pharmacophores derived from molecular dynamics simulations, Int. J. Mol. Sci. 21 (18) (2020) 6898, https://doi.org/10.3390/ijms21186898.

[29] J. Dernovšek, Ž. Zajec, M. Durcik, L.P. Mašič, M. Gobec, N. Zidar, T. Tomašič, Structure-activity relationships of benzothiazole-based Hsp90 C-terminal-domain inhibitors, Pharmaceutics 13 (8) (2021) 1283, https://doi.org/10.3390/pharmaceutics13081283.

[30] Ž. Zajec, J. Dernovšek, M. Gobec, T. Tomašič, In silico discovery and optimisation of a novel structural class of Hsp90 C-terminal domain inhibitors, Biomolecules 12 (7) (2022) 884, https://doi.org/10.3390/biom12070884.

[31] A.E. Cotman, P.A. Dub, M. Sterle, M. Lozinšek, J. Dernovšek, Ž. Zajec, A. Zega, T. Tomašič, D. Cahard, Catalytic stereoconvergent synthesis of homochiral β-CF3, β-SCF3, and β-OCF3 benzylic alcohols, ACS Org. Inorg. Au (2022), https://doi.org/10.1021/acsorginorgau.2c00019.

[32] Ž. Zajec, J. Dernovšek, M. Distel, M. Gobec, T. Tomašič, Optimisation of pyrazolo [1,5-*a*]pyrimidin-7(4*H*)-one derivatives as novel Hsp90 C-terminal domain inhibitors against Ewing sarcoma, Bioorg. Chem. 131 (2023) 106311, https://doi.org/10.1016/j.bioorg.2022.106311.

[33] Ž. Zajec, J. Dernovšek, J. Cingl, I. Ogris, M. Gedgaudas, A. Zubrienė, A. Mitrović, S. Golič Grdadolnik, M. Gobec, T. Tomašič, New class of Hsp90 C-terminal domain inhibitors with anti-tumor properties against triple-negative breast cancer, J. Med. Chem. (2024), https://doi.org/10.1021/acs.jmedchem.4c00932.

[34] J. Dernovšek, T. Tomašič, Following the design path of isoform-selective Hsp90 inhibitors: small differences, great opportunities, Pharmacol. Ther. 245 (2023) 108396, https://doi.org/10.1016/j.pharmthera.2023.108396.

[35] J. Yu, C. Zhang, C. Song, Pan- and Isoform-specific inhibition of Hsp90: design strategy and recent advances, Eur. J. Med. Chem. 238 (2022) 114516, https://doi.org/10.1016/j.ejmech.2022.114516.

[36] S. Bhatia, L. Spanier, D. Bickel, N. Dienstbier, V. Woloschin, M. Vogt, H. Pols, B. Lungerich, J. Reiners, N. Aghaallaei, D. Diedrich, B. Frieg, J. Schliehe-Diecks, B. Bopp, F. Lang, M. Gopalswamy, J. Loschwitz, B. Bajohgli, J. Skokowa, A. Borkhardt, J. Hauer, F.K. Hansen, S.H.J. Smits, J. Jose, H. Gohlke, T. Kurz, Development of a first-in-class small-molecule inhibitor of the C-terminal Hsp90 dimerization, ACS Cent. Sci. 8 (5) (2022) 636–655, https://doi.org/10.1021/acscentsci.2c00013.

[37] F.V. Stanger, C. Dehio, T. Schirmer, Structure of the N-terminal gyrase B fragment in complex with ADP·Pi reveals rigid-body motion induced by ATP hydrolysis, PLoS One 9 (9) (2014) e107289, https://doi.org/10.1371/journal.pone.0107289.

[38] K.A. Verba, R.-Y.-R. Wang, A. Arakawa, Y. Liu, M. Shirouzu, S. Yokoyama, D. A. Agard, Atomic structure of Hsp90-Cdc37-Cdk4 reveals That Hsp90 traps and stabilizes an unfolded kinase, Science 352 (6293) (2016) 1542–1547, https://doi.org/10.1126/science.aaf5023.

[39] T.G.P. Grünewald, F. Cidre-Aranaz, D. Surdez, E.M. Tomazou, E. de Álava, H. Kovar, P.H. Sorensen, O. Delattre, U. Dirksen, Ewing sarcoma, Nat. Rev. Dis. Primer 4 (1) (2018) 5, https://doi.org/10.1038/s41572-018-0003-x.

[40] S.R. Ambati, E.C. Lopes, K. Kosugi, U. Mony, A. Zehir, S.K. Shah, T. Taldone, A. L. Moreira, P.A. Meyers, G. Chiosis, M.A.S. Moore, Pre-clinical efficacy of PU-H71, a novel HSP90 inhibitor, alone and in combination with bortezomib in Ewing sarcoma, Mol. Oncol. 8 (2) (2014) 323–336, https://doi.org/10.1016/j.molonc.2013.12.005.

[41] E. Destanovic, J. Boos, C. Lanvers-Kaminsky, Preclinical evaluation of combined topoisomerase and proteasome inhibition against pediatric malignancies, Anticancer Res 38 (7) (2018) 3977–3984. 10.21873/anticanres.12684.

[42] D. Fayzullina, S. Tsibulnikov, M. Stempen, B.A. Schroeder, N. Kumar, R. K. Kharwar, A. Acharya, P. Timashev, I. Ulasov, Novel targeted therapeutic strategies for Ewing sarcoma, Cancers 14 (8) (2022) 1988, https://doi.org/10.3390/cancers14081988.

[43] J. Dernovšek, Ž. Zajec, G. Poje, D. Urbančič, C. Sturtzel, T. Goričan, S. Grissenberger, K. Ciura, M. Woziński, M. Gedgaudas, A. Zubrienė, S. G. Grdadolnik, I. Mlinarič-Raščan, Z. Rajić, A.E. Cotman, N. Zidar, M. Distel, T. Tomašič, Exploration and optimisation of structure-activity relationships of new triazole-based C-terminal Hsp90 inhibitors towards *in Vivo* anticancer potency, Biomed. Pharmacother. 177 (2024) 116941, https://doi.org/10.1016/j.biopha.2024.116941.

[44] P. Lassalas, B. Gay, C. Lasfargeas, M.J. James, V. Tran, K.G. Vijayendran, K. R. Brunden, M.C. Kozlowski, C.J. Thomas, A.B.I. Smith, D.M. Huryn, C. Ballatore, Structure property relationships of carboxylic acid isosteres, J. Med. Chem. 59 (7) (2016) 3183–3203, https://doi.org/10.1021/acs.jmedchem.5b01963.

[45] W. Chen, J. Qiu, Y. Shen, Topoisomerase IIα, rather than IIβ, is a promising target in development of anti-cancer drugs, Drug Discov. Ther. 6 (5) (2012) 230–237, https://doi.org/10.5582/ddt.2012.v6.5.230.
[46] E.J. Walsby, S.J. Coles, S. Knapper, A.K. Burnett, The topoisomerase II inhibitor voreloxin causes cell cycle arrest and apoptosis in myeloid leukemia cells and acts in synergy with cytarabine, Haematologica 96 (3) (2011) 393–399, https://doi.org/10.3324/haematol.2010.032680.
[47] B. Cao, H. Chen, Y. Gao, C. Niu, Y. Zhang, L. Li, CIP-36, a novel topoisomerase II-targeting agent, induces the apoptosis of multidrug-resistant cancer cells in vitro, Int. J. Mol. Med. 35 (3) (2015) 771–776, https://doi.org/10.3892/ijmm.2015.2068.
[48] J. Okamoto, I. Mikami, Y. Tominaga, K.M. Kuchenbecker, Y.-C. Lin, D.T. Bravo, G. Clement, A. Yagui-Beltran, M.R. Ray, K. Koizumi, B. He, D.M. Jablons, Inhibition of Hsp90 leads to cell cycle arrest and apoptosis in human malignant pleural mesothelioma, J. Thorac. Oncol. 3 (10) (2008) 1089–1095, https://doi.org/10.1097/JTO.0b013e3181839693.
[49] J.M. Park, Y.-J. Kim, S. Park, M. Park, L. Farrand, C.-T. Nguyen, J. Ann, G. Nam, H.-J. Park, J. Lee, J.Y. Kim, J.H. Seo, A novel HSP90 inhibitor targeting the C-terminal domain attenuates trastuzumab resistance in HER2-positive breast cancer, Mol. Cancer 19 (1) (2020) 161, https://doi.org/10.1186/s12943-020-01283-6.
[50] A.K. Samadi, X. Zhang, R. Mukerji, A.C. Donnelly, B.S. Blagg, M.S. Cohen, A novel C-terminal HSP90 inhibitor KU135 induces apoptosis and cell cycle arrest in melanoma cells, Cancer Lett. 312 (2) (2011) 158–167, https://doi.org/10.1016/j.canlet.2011.07.031.
[51] P.K. Karkoulis, D.J. Stravopodis, E.G. Konstantakou, G.E. Voutsinas, Targeted inhibition of heat shock protein 90 disrupts multiple oncogenic signaling pathways, thus inducing cell cycle arrest and programmed cell death in human urinary bladder cancer cell lines, Cancer Cell Int. 13 (1) (2013) 11, https://doi.org/10.1186/1475-2867-13-11.
[52] S. Mitra, B. Ghosh, N. Gayen, J. Roy, A.K. Mandal, Bipartite role of heat shock protein 90 (Hsp90) keeps CRAF kinase poised for activation, J. Biol. Chem. 291 (47) (2016) 24579–24593, https://doi.org/10.1074/jbc.M116.746420.
[53] C. Sturtzel, S. Grissenberger, P. Bozatzi, E. Scheuringer, A. Wenninger-Weinzierl, Z. Zajec, J. Dernovšek, S. Pascoal, V. Gehl, A. Kutsch, A. Granig, F. Rifatbegovic, M. Carre, A. Lang, I. Valtingojer, J. Moll, D. Lötsch, F. Erhart, G. Widhalm, D. Surdez, O. Delattre, N. André, J. Stampfl, T. Tomašič, S. Taschner-Mandl, M. Distel, Refined high-content imaging-based phenotypic drug screening in zebrafish xenografts, npj Precis. Oncol. 7 (1) (2023) 1–16, https://doi.org/10.1038/s41698-023-00386-9.
[54] J.C. Shelley, A. Cholleti, L.L. Frye, J.R. Greenwood, M.R. Timlin, M. Uchimaya, Epik: a software program for pKa prediction and protonation state generation for drug-like molecules, J. Comput. Aided Mol. Des. 21 (12) (2007) 681–691, https://doi.org/10.1007/s10822-007-9133-z.
[55] K.J. Bowers, E. Chow, H. Xu, R.O. Dror, M.P. Eastwood, B.A. Gregersen, J. L. Klepeis, I. Kolossvary, M.A. Moraes, F.D. Sacerdoti, J.K. Salmon, Y. Shan, D. E. Shaw, Scalable algorithms for molecular dynamics simulations on commodity clusters, in: Proceedings of the 2006 ACM/IEEE conference on Supercomputing; SC'06, Association for Computing Machinery, New York, NY, USA, 2006, p. 84-es, https://doi.org/10.1145/1188455.1188544.
[56] W.L. Jorgensen, D.S. Maxwell, J. Tirado-Rives, Development and testing of the OPLS all-atom force field on conformational energetics and properties of organic liquids, J. Am. Chem. Soc. 118 (45) (1996) 11225–11236, https://doi.org/10.1021/ja9621760.
[57] M. Gedgaudas, D. Baronas, E. Kazlauskas, V. Petrauskas, D. Matulis, Thermott: a comprehensive online tool for protein-ligand binding constant determination, Drug Discov. Today 27 (8) (2022) 2076–2079, https://doi.org/10.1016/j.drudis.2022.05.008.
[58] T.L. Hwang, A.J. Shaka, Water suppression that works. Excitation sculpting using arbitrary wave-forms and pulsed-field gradients, J. Magn. Reson. A 112 (2) (1995) 275–279, https://doi.org/10.1006/jmra.1995.1047.
[59] M. Mayer, B. Meyer, Group epitope mapping by saturation transfer difference NMR to identify segments of a ligand in direct contact with a protein receptor, J. Am. Chem. Soc. 123 (25) (2001) 6108–6117, https://doi.org/10.1021/ja0100120.
[60] J. Yan, A.D. Kline, H. Mo, M.J. Shapiro, E.R. Zartler, The effect of relaxation on the epitope mapping by saturation transfer difference NMR, J. Magn. Reson. 163 (2) (2003) 270–276, https://doi.org/10.1016/S1090-7807(03)00106-X.
[61] C. McCullough, M. Wang, L. Rong, M. Caffrey, Characterization of influenza hemagglutinin interactions with receptor by NMR, PLoS One 7 (7) (2012) e33958, https://doi.org/10.1371/journal.pone.0033958.
[62] G.M. Clore, A.M. Gronenborn, Theory and applications of the transferred nuclear overhauser effect to the study of the conformations of small ligands bound to proteins, J. Magn. Reson. 1969 48 (3) (1982) 402–417, https://doi.org/10.1016/0022-2364(82)90073-7.